AIMS Mathematics, 11(8): 26834–26867.
DOI: 10.3934/math.20261077
Received: 13 June 2026
Revised: 09 August 2026
Accepted: 19 August 2026
Published: 26 August 2026

http://www.aimspress.com/journal/Math

Research article

A network reaction–transport model for Ebola dynamics with adaptive mobility, spillover, and behavioral feedback

Olumuyiwa James Peter[1,2,*], Azhar Iqbal Kashif Butt[3,*], Sharifah Sakinah Syed Ahmad[4], and Muneerah AL Nuwairan[3]

[1] Department of Mathematics, Saveetha School of Engineering, SIMATS, Saveetha University, Chennai, Tamil Nadu, India

[2] Department of Mathematical and Computer Sciences, University of Medical Sciences, Ondo City, Ondo State, Nigeria

[3] Department of Mathematics and Statistics, College of Science, King Faisal University, Al-Ahsa 31982, Saudi Arabia

[4] Faculty of Artificial Intelligence and Cyber Security, Universiti Teknikal Malaysia Melaka, Malaysia

* **Correspondence:** Email: peterjames4real@gmail.com, aikhan@kfu.edu.sa.

Abstract: Ebola virus disease is an ever-present threat to public health, driven by the interplay of zoonotic transmission, human mobility, high-risk social behaviors, and behavioral responses to infection. In the present work, we proposed and thoroughly analyzed a network-based reaction–transport model of Ebola virus disease transmission, which simultaneously accounts for the dynamics of adaptive human mobility, higher-order transmission, and zoonotic spillover. Our model precisely incorporates routine pairwise transmission, group transmission through funerals and healthcare settings, survivor relapse, and continuous reseeding from animal reservoirs, as well as human mobility responses to local prevalence through fear-based suppression. We rigorously proved the positivity, global boundedness, and well-posedness of the resulting nonlinear system, despite state-dependent transport and continuous external forcing. We derived a network-based basic reproduction number using an operator-theoretic next-generation method, which integrates transmission, recovery, and mobility-driven spatial transport. Our analysis precisely shows that zoonotic transmission fundamentally alters classical epidemic thresholds: in the subcritical human-to-human transmission regime, continuous reseeding invariably drives the system toward a positive endemic equilibrium. Using resolvent and spectral analysis, we meticulously demonstrated the anti-diffusive effect of fear-based mobility suppression, which generates spatial trapping, hysteresis, eigenvector localization, and Turing-type instabilities leading to the formation of geographically localized and persistent Ebola virus disease hotspots. Numerical simulations on synthetic mobility networks confirmed the theoretical results and thoroughly demonstrated sharp

phase transitions governing hotspot dominance and persistence. Our results rigorously showed that zoonotic transmission controls the persistence of Ebola Virus Disease, while mobility and behavioral responses determine the spatial localization of the endemic equilibrium. Overall, this work provides a mechanistic explanation for the observed coexistence of low global prevalence and strong spatial localization of Ebola Virus Disease and offers new insight into the complex interplay among behavioral responses, network structure, and zoonotic transmission.

Keywords: Ebola virus; zoonotic spillover; adaptive human mobility; network reaction–transport models; fear-driven behavior; spatial heterogeneity; nonlinear transmission
Mathematics Subject Classification: 91A40, 34D23

1. Introduction

Ebola virus disease (EVD), also known as Ebola, is a severe zoonotic infection caused by viruses of the genus *Ebolavirus*, which have been responsible for the disease since its initial outbreaks in Central Africa in 1976 [1, 2]. The contagiousness and severity of this condition are extremely high, with rapid onset, high viral loads, and case fatality rates that have ranged between approximately 25% and 70%, depending on the outbreak [2, 3]. Transmission occurs primarily through direct contact with infected bodily fluids, contaminated materials, and deceased individuals, making caregiving and funeral practices major contributing factors to epidemic spread [4, 5].

The West African outbreak, which lasted from 2013 to 2016, drastically changed the global understanding of Ebola virus disease. This epidemic resulted in more than 28,000 reported infections and over 11,000 deaths [2]. Unlike earlier outbreaks, which were typically localized and self-limiting, the West African epidemic was not confined to a single geographical region and exhibited sustained transmission across national borders [6]. Since then, the Democratic Republic of the Congo has experienced several Ebola outbreaks, reinforcing the conclusion that Ebola remains a persistent underlying threat, particularly in regions where ecological and environmental conditions are favorable for viral spillover and transmission [7, 8].

Ecological studies have confirmed that Ebola virus continues to circulate within animal populations, with fruit bats widely recognized as likely long-term reservoir hosts [9, 10]. Spillover events from animals to humans are relatively rare but play a critical role in initiating and sustaining outbreaks, particularly in forested and rural regions where close contact between human and wildlife populations is common [8]. Even after outbreaks appear to be fully controlled, reintroduction of the virus can occur, complicating eradication efforts through repeated zoonotic spillover events [11].

Mathematical modeling has played a central role in elucidating Ebola transmission dynamics and informing outbreak response strategies. One of the most influential deterministic models was proposed by Legrand et al. [12], in which Ebola transmission was decomposed into three distinct pathways: community, hospital, and funeral settings, allowing estimation of their relative contributions to epidemic growth. Subsequent modeling studies introduced additional structural complexity, including nonlinear incidence functions and expanded epidemiological compartments, to better reproduce observed outbreak dynamics [13, 14]. During the 2014–2016 West African epidemic,

mathematical models were extensively used to estimate key epidemiological quantities, such as the basic reproduction number R_0, and to evaluate the potential impact of intervention strategies including isolation, contact tracing, and strengthened healthcare system responses [15–17].

For the computation of the basic reproduction number in general structured population models, from both analytical and numerical perspectives, see, for example, Barril et al. [18] and Breda et al. [19]. More broadly, mathematical epidemic models have been used to characterize transmission dynamics, estimate epidemiological quantities, and investigate epidemic trends across different infectious diseases [20, 21].

Spatial and network-based models have expanded traditional compartmental frameworks by explicitly incorporating human mobility between geographically distinct regions. This extension enables assessment of the spatial progression of epidemics and evaluation of the potential impact of travel restrictions on disease spread [22, 23].

In the context of Ebola, reviews of mathematical modeling approaches emphasize the wide spectrum of methods applied, ranging from simple susceptible-infected-recovered (SIR)-type frameworks to more complex stochastic and spatially explicit models. These reviews also highlight the critical importance of linking models to field-collected observational data and real-time outbreak analytics in order to improve model relevance and reliability [24, 25].

More recently, advanced modeling approaches have incorporated delay differential equations, optimal control theory, and fractional-order frameworks to account for incubation delays, resource constraints, and memory effects in Ebola transmission dynamics [16].

During the West African outbreak, researchers employed a broad range of deterministic and stochastic models to estimate key epidemiological parameters, including the basic reproduction number and the generation interval, as well as to forecast the future trajectory of the epidemic [15, 16]. Across these studies, it was consistently shown that timely isolation, safe burial practices, and extensive contact tracing were, in principle, capable of reducing transmission below the threshold required for sustained spread [23, 26].

With specific emphasis on geography and network structure, several modeling approaches demonstrated the critical role of human mobility in driving Ebola transmission. Meta-population models analyzing movement between geographically distinct regions were used to assess the risk of international spread and to evaluate how travel restrictions could influence epidemic dynamics [22, 23]. Analyses incorporating empirical mobility data derived from mobile phone records further showed that reductions in human movement during outbreaks led to substantial changes in the spatiotemporal patterns of Ebola spread [27].

Behavioral responses to Ebola outbreaks are increasingly incorporated into mathematical modeling studies. As individuals become informed and fearful, their perception of risk changes, leading to reductions in contact rates, avoidance of high-incidence areas, and delays or alterations in healthcare-seeking behavior [28, 29]. Such feedback mechanisms naturally generate non-exponential epidemic growth and strongly influence both the size and the geographic extent of outbreaks [30].

Recent reaction-diffusion models have revealed that spatial heterogeneity and nonlinear transmission can induce the formation of localized disease hotspots [31]. Network-based research has shown that higher-order transmission causes diffusion-driven pattern creation and geographic localization of epidemics [32]. Adaptive mobility plays a significant role in disease propagation, as demonstrated in spatial cholera and Mpox models [33, 34]. Fractional-order formulations have shed

light on the dynamics of zoonotic illnesses like Lassa fever [35]. These findings support the current reaction–transport framework for studying the combined effects of adaptive mobility, behavioral feedback, and persistent zoonotic spillover on Ebola transmission.

Nevertheless, several gaps remain. Most existing models treat human mobility as fixed or externally prescribed, rather than as a dynamic process that responds endogenously to infection prevalence. Large transmission events, including funerals and hospital ward exposures, are frequently approximated by simple pairwise contacts, thereby obscuring their collective and group-level nature [13]. Finally, few models incorporate spatially heterogeneous zoonotic spillover within a mass-conserving network framework, limiting understanding of how ecological drivers and behavioral responses jointly shape long-term Ebola persistence.

Thus, motivated by the need to understand how behavioral responses, ecological forcing, and network structure jointly shape Ebola persistence, we introduce a spatially explicit *network-based reaction–transport framework*. This framework unifies adaptive human mobility, higher-order transmission processes, and persistent zoonotic spillover within a single Eulerian formulation. To our knowledge, this study is the first to:

- develop a Eulerian, network-based reaction–transport model of Ebola transmission in which all epidemiological compartments represent individuals physically present at each network node, allowing mobility, contact, and spillover to operate within a common spatial frame;
- incorporate fear-driven adaptive mobility into a mass-conserving transport operator, where diffusion rates depend nonlinearly on local infection prevalence and dynamically suppress departures from highly infected nodes while preserving total population under movement;
- establish a nonlinear feedback loop between epidemic prevalence and spatial transport on networks, demonstrating how behavioral responses deform diffusion operators and generate mobility-induced trapping;
- extend higher-order (group-level) transmission mechanisms by introducing a network-mediated aggregation operator to represent funerals and healthcare settings, capturing how participants arriving from multiple nodes amplify local transmission risk;
- explicitly include spatially heterogeneous zoonotic spillover as a persistent external forcing term, enabling analysis of wildlife-driven reseeding that sustains endemic infection and selects hotspot locations even when human-to-human transmission is subcritical;
- establish well-posedness, positivity, and global boundedness of the full nonlinear reaction–transport system despite state-dependent mobility and continual spillover, ensuring both biological and mathematical consistency;
- derive a network-level basic reproduction number using an operator-theoretic next-generation formulation that jointly accounts for transmission, recovery, and mobility-driven spatial circulation;
- demonstrate analytically that zoonotic spillover removes classical eradication thresholds, replacing disease-free stability with spillover-driven endemic equilibria governed by operators on the mobility network;
- perform operator-level spectral analysis showing how fear-induced mobility suppression generates anti-diffusive effects, leading to eigenvector localization and Turing-like instabilities on networks;
- numerically identify phase transitions in Ebola spatial organization, revealing how baseline

mobility controls hotspot multiplicity, spillover governs persistence, and behavioral feedback determines the dominance and localization of endemic reservoirs.

This study accomplishes this by combining adaptive human mobility, higher-order social transmission, and multiple animal-to-human forcing mechanisms within a rigorously mass-conserving framework, moving beyond traditional Ebola models that treat mobility, behavior, and spillover as independent or static processes. This provides new theoretical perspectives for mechanistically understanding the formation of endemic hotspots without external intervention, how fear can spatially anchor outbreaks, and how Ebola persists locally over extended time horizons. In doing so, the framework addresses longstanding questions regarding why Ebola outbreaks remain geographically localized yet episodically recurrent, even in the presence of behavioral avoidance and subcritical transmission.

The proposed approach establishes a robust mathematical foundation for studying the combined effects of adaptive human mobility, higher-order transmission, and persistent zoonotic spillover on the spatial dynamics of Ebola virus disease. The model builds on prior Ebola transmission models by incorporating these mechanisms into a mass-conserving network reaction–transport framework, rather than treating mobility, behavioral responses, or ecological spillover in isolation. The analytical findings show how fear-driven mobility suppression affects epidemic thresholds, promotes spatial trapping, and leads to the establishment and persistence of spatially limited endemic hotspots. Complementary numerical models demonstrate how mobility, spillover intensity, and network structure influence the long-term geographical organization of Ebola outbreaks. In addition to offering a mathematical framework for evaluating intervention strategies that concurrently target human mobility, behavioral adaptation, and zoonotic transmission, these findings collectively offer new theoretical insight into the mechanisms underlying the recurrent but geographically localized nature of Ebola epidemics. The rest of the paper is organized as follows. Section 2 outlines the proposed Ebola reaction–transport model and associated biological assumptions. Section 3 defines the model's main mathematical aspects, such as positivity, boundedness, network reproduction number, spillover-driven persistence, and hotspot localization. Section 4 examines fear-induced spatial instability and pattern creation using operator-theoretic analysis. Section 5 includes numerical simulations that demonstrate the impact of adaptive mobility, behavioral feedback, and zoonotic spillover on Ebola dynamics. Section 6 summarizes key findings, discusses their epidemiological consequences, and suggests future study possibilities.

2. Model formulation

Ebola virus disease is a sudden and often fatal viral hemorrhagic illness that occurs following contact with infected bodily fluids, contaminated objects, or infected animals, particularly fruit bats and nonhuman primates. Ebola outbreaks are typically spatially localized, are amplified by high-risk activities such as caregiving and funeral practices, and are sustained through repeated spillover events from animal reservoirs and infected individuals. The central premise is that zoonotic spillover continually reintroduces infection into human populations, thereby triggering and maintaining outbreaks. Motivated by this mechanism, we develop a Eulerian, network-structured reaction–transport model in which each epidemiological compartment represents individuals who are physically present at specific spatial locations.

2.1. Network structure and population states

Each of the N nodes in our connected network represents a community, district, or healthcare catchment region. A weighted undirected graph with symmetric edge weights $w_{ij} = w_{ji} \geq 0$ describes human mobility across nodes. Let $S_i(t)$, $I_i(t)$, and $R_i(t)$ represent the susceptible, infected, and recovered (Ebola survivor) populations *present at node* i at time t. At node i, the entire population is

$$N_i(t) = S_i(t) + I_i(t) + R_i(t). \tag{2.1}$$

2.2. Transmission mechanisms

Ebola spreads through three biologically different routes.

Pairwise human-to-human transmission. Routine close encounters, such as caring and hospitalization, take place locally among individuals physically present at the same node. Thus, pairwise transmission generates new infections at node i at a rate of

$$\beta_1 S_i \frac{I_i}{N_i}. \tag{2.2}$$

Funeral and healthcare group transmission. Funerals and hospital wards are two high-risk group events that are spatially located at node i. Let $\tilde{A}^{(2)}_{ik}$ represent the strength of interaction between persons at node i and those coming from node k to participate in such gatherings. The group infection term is

$$\beta_2 S_i \sum_{k=1}^{N} \tilde{A}^{(2)}_{ik} \frac{I_k}{N_k}. \tag{2.3}$$

Here, $\tilde{A}^{(2)} = (\tilde{A}^{(2)}_{ik})$ is a nonnegative interaction matrix whose entry $\tilde{A}^{(2)}_{ik}$ represents the relative intensity of high-risk group interactions between infected individuals originating from node k and gatherings occurring at node i, such as funerals or healthcare settings. Larger values of $\tilde{A}^{(2)}_{ik}$ correspond to stronger opportunities for group transmission, whereas $\tilde{A}^{(2)}_{ik} = 0$ indicates no such interaction. This formulation represents the exposure of susceptibles at node i to infected individuals arriving from all nodes k, including $k = i$, while avoiding double counting and residence-based normalization.

Zoonotic spillover. Ecological transmission from wildlife reservoirs at node i produces $\lambda_i S_i$, acting on all individuals physically present at node i.

2.3. Survivor-mediated relapse

Recovered individuals may relapse and become infectious: $R_i \xrightarrow{\omega} I_i$.

For analytical tractability, the zoonotic spillover rate λ_i and the survivor relapse rate ω are assumed to be constant throughout the study period. Although seasonal spillover and time-dependent relapse may influence Ebola transmission, incorporating these processes requires detailed ecological and epidemiological data, and is beyond the scope of the present study.

2.4. Local reaction dynamics

The epidemiological dynamics at node i are

$$\frac{dS_i}{dt} = B_i - \eta S_i - \beta_1 S_i \frac{I_i}{N_i} - \beta_2 S_i \sum_{k=1}^{N} \tilde{A}_{ik}^{(2)} \frac{I_k}{N_k} - \lambda_i S_i, \tag{2.4}$$

$$\frac{dI_i}{dt} = \beta_1 S_i \frac{I_i}{N_i} + \beta_2 S_i \sum_{k=1}^{N} \tilde{A}_{ik}^{(2)} \frac{I_k}{N_k} + \lambda_i S_i + \omega R_i - (\gamma + \eta + \delta) I_i, \tag{2.5}$$

$$\frac{dR_i}{dt} = \gamma I_i - (\eta + \omega) R_i. \tag{2.6}$$

2.5. Fear-driven adaptive mobility

Let

$$\rho_i(t) = \frac{I_i(t)}{N_i(t)} \tag{2.7}$$

represent local prevalence. Fear suppresses outgoing travel from infected nodes via a smooth mobility function

$$d_i = d(\rho_i) = \frac{d_b}{1 + \exp\left[a(\rho_i - \theta)\right]}, \tag{2.8}$$

where d_b is the baseline mobility, θ is the fear threshold, and a controls the sharpness of the behavioral response.

2.6. Mass-conserving transport operator

For any compartment $X_i \in \{S_i, I_i, R_i\}$, mobility is governed by the mass-conserving operator

$$\sum_{j=1}^{N} w_{ij}(d_j X_j - d_i X_i). \tag{2.9}$$

This operator reduces movement from high-prevalence nodes while conserving the total population under transit.

2.7. Full reaction–transport system

$$\frac{dS_i}{dt} = \sum_{j=1}^{N} w_{ij}(d_j S_j - d_i S_i) + B_i - \eta S_i - \beta_1 S_i \frac{I_i}{N_i} - \beta_2 S_i \sum_{k=1}^{N} \tilde{A}_{ik}^{(2)} \frac{I_k}{N_k} - \lambda_i S_i. \tag{2.10}$$

$$\frac{dI_i}{dt} = \sum_{j=1}^{N} w_{ij}(d_j I_j - d_i I_i) + \beta_1 S_i \frac{I_i}{N_i} + \beta_2 S_i \sum_{k=1}^{N} \tilde{A}_{ik}^{(2)} \frac{I_k}{N_k} + \lambda_i S_i + \omega R_i - (\gamma + \eta + \delta) I_i. \tag{2.11}$$

$$\frac{dR_i}{dt} = \sum_{j=1}^{N} w_{ij}(d_j R_j - d_i R_i) + \gamma I_i - (\eta + \omega) R_i. \tag{2.12}$$

2.8. Model assumptions

- All epidemiological variables indicate persons who are physically present at each node (Euler framework). Zoonotic spillover affects all individuals present at a node.
- Group transmission happens through spatially localized meetings of arriving individuals. Fear reduces outward mobility in a smooth and consistent manner.
- Transport preserves total population mass but births and deaths do not. The model variables and parameters are presented in Table 1.

Table 1. Model parameters and variables for the spatial Ebola reaction–transport system.

Symbol	Units	Meaning
$S_i(t)$	people	Number of susceptible individuals physically present at node i
$I_i(t)$	people	Number of infectious individuals physically present at node i
$R_i(t)$	people	Recovered (Ebola survivor) individuals present at node i
$N_i(t)$	people	Total population present at node i
β_1	time^{-1}	Rate of transmission for routine pairwise human-to-human contact
β_2	time^{-1}	Transmission rate for high-risk group settings (funerals, hospital wards)
$\tilde{A}^{(2)}_{ik}$	dimensionless	Strength of participation of individuals from node k in group events at node i
λ_i	time^{-1}	Zoonotic spillover rate at node i
γ	time^{-1}	Recovery rate from Ebola infection
δ	time^{-1}	Ebola-induced mortality rate
ω	time^{-1}	Relapse rate of recovered survivors back to the infectious state
η	time^{-1}	Natural (non-Ebola) mortality rate
B_i	people time^{-1}	Recruitment (birth or immigration) rate at node i
w_{ij}	time^{-1}	Baseline mobility rate between nodes i and j
d_b	dimensionless	Baseline probability of travel per unit time
a	dimensionless	Steepness of fear response to prevalence
θ	dimensionless	Prevalence threshold triggering mobility suppression
$d_i(\rho_i)$	dimensionless	Effective mobility at node i as a function of prevalence
$\rho_i(t)$	dimensionless	Local prevalence at node i, $\rho_i = I_i/N_i$

Remark 1. The prevalence-dependent mobility function is intended to represent the aggregate effects of individual risk perception, government-imposed public-health interventions, travel restrictions, and other behavioral adaptations that influence human movement during Ebola outbreaks. Rather than

modeling each of these mechanisms explicitly, they are incorporated into a single prevalence-dependent mobility function to maintain mathematical tractability while capturing the essential feedback between disease prevalence and population movement.

3. Mathematical analysis of the Ebola reaction–transport model

In this part, we investigate the reaction–transport system Eqs (2.10)–(2.12) to determine if the model is mathematically well-posed, if Ebola may enter the geographical network, and how spillover, mobility, and fear affect long-term persistence. We first demonstrate that solutions are biologically relevant (positive and bounded). We then establish a baseline disease-free spatial state, investigate early invasion using a network reproduction number, and demonstrate how spillover and anxiety build persistent endemic hotspots.

3.1. Positivity and boundedness

Positivity. Assume nonnegative initial conditions

$$S_i(0) \geq 0, \qquad I_i(0) \geq 0, \qquad R_i(0) \geq 0, \qquad i = 1, \ldots, N.$$

According to the reaction–transport system equations (2.10)–(2.12), gain terms in each compartment are nonnegative when state variables are nonnegative, and loss terms are proportional to the state itself. Moreover, the transportation operator

$$\sum_{j=1}^{N} w_{ij}(d_j X_j - d_i X_i), \qquad X \in \{S, I, R\},$$

is mass-conserving and cannot generate negative values.

Therefore:

- If $S_i = 0$, then all loss terms vanish and $\dot{S}_i \geq 0$;
- If $I_i = 0$, then $\dot{I}_i = \lambda_i S_i + \omega R_i \geq 0$;
- If $R_i = 0$, then $\dot{R}_i = \gamma I_i \geq 0$.

Hence, the positive orthant is forward invariant, and

$$S_i(t) \geq 0, \qquad I_i(t) \geq 0, \qquad R_i(t) \geq 0, \qquad \forall t \geq 0, \quad i = 1, \ldots, N. \tag{3.1}$$

Total population dynamics. Define the total population at node i by $N_i = S_i + I_i + R_i$.

By combining Eqs (2.10)–(2.12), all infection, recovery, relapse, and spillover terms cancel out, producing

$$\frac{dN_i}{dt} = \sum_{j=1}^{N} w_{ij}(d_j N_j - d_i N_i) + B_i - \eta N_i - \delta I_i. \tag{3.2}$$

Summing over all nodes i gives

$$\frac{d}{dt}\sum_{i=1}^{N} N_i = \sum_{i=1}^{N}\sum_{j=1}^{N} w_{ij}(d_j N_j - d_i N_i) + \sum_{i=1}^{N} B_i - \eta \sum_{i=1}^{N} N_i - \delta \sum_{i=1}^{N} I_i. \tag{3.3}$$

Because $w_{ij} = w_{ji}$, the transport term vanishes by symmetry:

$$\sum_{i=1}^{N}\sum_{j=1}^{N} w_{ij}(d_j N_j - d_i N_i) = 0.$$

Therefore,

$$\frac{d}{dt}\sum_{i=1}^{N} N_i = \sum_{i=1}^{N} B_i - \eta \sum_{i=1}^{N} N_i - \delta \sum_{i=1}^{N} I_i. \tag{3.4}$$

Since $I_i \geq 0$,

$$\frac{d}{dt}\sum_{i=1}^{N} N_i \leq \sum_{i=1}^{N} B_i - \eta \sum_{i=1}^{N} N_i. \tag{3.5}$$

Let

$$N(t) = \sum_{i=1}^{N} N_i(t), \qquad B = \sum_{i=1}^{N} B_i.$$

Then

$$\frac{dN}{dt} \leq B - \eta N.$$

By the comparison principle,

$$N(t) \leq N(0)e^{-\eta t} + \frac{B}{\eta}\left(1 - e^{-\eta t}\right), \qquad t \geq 0. \tag{3.6}$$

Consequently,

$$\boxed{\sum_{i=1}^{N} N_i(t) \leq \max\left\{\sum_{i=1}^{N} N_i(0), \frac{\sum_{i=1}^{N} B_i}{\eta}\right\}, \qquad t \geq 0.} \tag{3.7}$$

Thus, the total population remains uniformly bounded for all $t \geq 0$. Hence, the spatial Ebola reaction–transport system is globally bounded, despite mobility and continuous zoonotic spillover. After establishing positivity and boundedness, we select the baseline spatial state against which Ebola invasion is evaluated.

3.2. Quasi-disease-free spatial equilibrium (DFSE)

When $\lambda_i > 0$, the classical disease-free state $I_i = 0$ cannot be an equilibrium of the entire system due to zoonotic spillover, which creates an ongoing external source of infection at each node. Nonetheless, early invasion and threshold behavior must be defined in relation to the underlying geographical population distribution that exists prior to epidemic transmission being active. This motivates the establishment of a baseline reference state achieved by reducing infection and relapse while preserving demography and mobility. We define the quasi-disease-free spatial equilibrium (DFSE) as the system's limiting state in the absence of infection and relapse:

$$I_i = 0, \qquad R_i = 0, \qquad S_i = S_i^*, \qquad i = 1, \ldots, N.$$

At this point, the local prevalence is $\rho_i = 0$, indicating that fear is absent and mobility has reached its baseline value of $d_i = d_b$. Substituting into the susceptibility equation of the complete reaction–transport system produces the linear network balance equation:

$$\sum_{j=1}^{N} w_{ij}(d_b S_j^* - d_b S_i^*) + B_i - \eta S_i^* = 0, \qquad i = 1, \ldots, N.$$

This system represents the network-wide equilibrium of demographic recruitment, natural mortality, and mobility-driven redistribution. Under normal connection assumptions, the mobility graph admits a singular positive solution $\{S_i^*\}$, representing the baseline geographic distribution of susceptible people in the absence of Ebola transmission.

The DFSE thus describes the demographic and mobility context into which Ebola seeks to infiltrate. All of the following linearization, reproduction number calculations, and persistence assessments are based on this quasi-disease-free spatial equilibrium.

3.3. Linearized invasion system

At the DFSE, prevalence satisfies $\rho_i = 0$ and thus $d_i = d_b$ for all nodes. Retaining only terms linear in I_i, Eq (2.11) becomes

$$\frac{dI_i}{dt} = \sum_{j=1}^{N} w_{ij}(d_b I_j - d_b I_i) + \beta_1 S_i^* \frac{I_i}{S_i^*} + \beta_2 S_i^* \sum_{k=1}^{N} \tilde{A}_{ik}^{(2)} \frac{I_k}{S_k^*} + \lambda_i S_i^* - (\gamma + \eta + \delta) I_i. \tag{3.8}$$

Since $N_i = S_i^*$ at the DFSE, this simplifies to

$$\frac{dI_i}{dt} = \sum_{j=1}^{N} w_{ij} d_b (I_j - I_i) + \beta_1 I_i + \beta_2 S_i^* \sum_{k=1}^{N} \tilde{A}_{ik}^{(2)} \frac{I_k}{S_k^*} - (\gamma + \eta + \delta) I_i + \lambda_i S_i^*. \tag{3.9}$$

Define the infected-state vector $\mathbf{I} = (I_1, \ldots, I_N)^T$, $\boldsymbol{\lambda} = (\lambda_1 S_1^*, \ldots, \lambda_N S_N^*)^T$.

We now introduce the linear operators:

Pairwise and group infection operator. Let $F \in \mathbb{R}^{N \times N}$ be defined by

$$F_{ik} = \beta_1 \delta_{ik} + \beta_2 S_i^* \frac{\tilde{A}_{ik}^{(2)}}{S_k^*}. \tag{3.10}$$

Transport operator. Let $T(d_b) \in \mathbb{R}^{N \times N}$ be the graph Laplacian weighted by baseline mobility,

$$T_{ik}(d_b) = d_b(w_{ik} - \delta_{ik} \sum_{j=1}^{N} w_{ij}). \tag{3.11}$$

Removal operator. Let $V \in \mathbb{R}^{N\times N}$ be the diagonal matrix

$$V_{ik} = (\gamma + \eta + \delta)\delta_{ik}. \tag{3.12}$$

With these definitions, the linearized Ebola invasion system takes the compact matrix form

$$\frac{d\mathbf{I}}{dt} = (F + T(d_b) - V)\mathbf{I} + \boldsymbol{\lambda}. \tag{3.13}$$

$F + T(d_b) - V$ is a forced network epidemic system governed by spatial amplification and diffusion of Ebola, while the constant forcing vector $\boldsymbol{\lambda}$ denotes continual reseeding from zoonotic spillover at each node.

3.4. Network reproduction number

Here, transmission, recovery, and mobility are combined into a single operator to generalize the traditional basic reproduction number to a network situation.

Examine the homogeneous linearized invasion system (spillover suppressed):

$$\frac{d\mathbf{I}}{dt} = (F + T(d_b) - V)\mathbf{I}. \tag{3.14}$$

Rearranging (3.14) gives

$$(V - T(d_b))\mathbf{I} = F\,\mathbf{I}. \tag{3.15}$$

Since V is a positive diagonal matrix and $T(d_b)$ is a conservative graph Laplacian, $V - T(d_b)$ is a nonsingular M-matrix and therefore invertible with a positive inverse. The associated next-generation operator is therefore defined by

$$\mathcal{K} = F\,(V - T(d_b))^{-1}. \tag{3.16}$$

The network basic reproduction number is

$$R_0 = \rho(\mathcal{K}), \tag{3.17}$$

where $\rho(\cdot)$ denotes the spectral radius.

This quantity incorporates:

- the mobility network through $T(d_b)$,
- spatial trapping and circulation of infection,
- pairwise and funeral transmission through F,
- heterogeneity in susceptible density via S_i^*.

When $R_0 < 1$, the disease-free spatial equilibrium is linearly stable in the absence of spillover.

3.5. Spillover-driven persistence

Even if the network reproduction number is below one, Ebola may persist because of continual zoonotic reseeding. Now consider the full forced invasion system:

$$\frac{d\mathbf{I}}{dt} = (F + T(d_b) - V)\mathbf{I} + \boldsymbol{\lambda}, \qquad \boldsymbol{\lambda} \geq 0. \tag{3.18}$$

Define $M = V - T(d_b) - F$. If $R_0 < 1$, then M is a nonsingular M-matrix. Consequently, $M^{-1} \geq 0$ exists.

The unique equilibrium of the forced system satisfies $M\,\mathbf{I}^* = \boldsymbol{\lambda}$, so

$$\mathbf{I}^* = M^{-1}\boldsymbol{\lambda}. \tag{3.19}$$

Since $M^{-1} \geq 0$ and $\boldsymbol{\lambda} \geq 0$, we have $\mathbf{I}^* \geq 0$, and moreover, $\mathbf{I}^* > 0$, whenever any $\lambda_i > 0$.

Therefore, even when $R_0 < 1$, in the presence of zoonotic reseeding, Ebola converges to a strictly positive endemic state, but the homogenous epidemic dynamics fade.

This demonstrates that ecological forcing takes the place of the classical elimination threshold: even if local transmission is subcritical, global eradication is impossible as long as external spillover is active at any node.

3.6. Hotspot localization

We will now describe how spatial structure influences where infection concentrates. At endemic equilibrium, the diseased state fulfills

$$(V - T(d_b) - F)\mathbf{I}^* = \boldsymbol{\lambda}. \tag{3.20}$$

Thus

$$\mathbf{I}^* = (V - T(d_b) - F)^{-1}\boldsymbol{\lambda}. \tag{3.21}$$

Because $V - T(d_b) - F$ is a nonsingular M-matrix when $R_0 < 1$, its inverse in (3.20) is positive and admits the resolvent expansion

$$(V - T - F)^{-1} = (V - T)^{-1} \sum_{n=0}^{\infty} \left(F(V - T)^{-1}\right)^n. \tag{3.22}$$

The resolvent $(V - T)^{-1}$ acts as a spatial Green function on the mobility network. Its entries decay with graph distance but are amplified by weak transport and slow removal. Therefore,

$$I_i^* = \sum_{j=1}^{N} (V - T - F)_{ij}^{-1}\,\lambda_j. \tag{3.23}$$

Equation (3.23) shows that infection at node i is a weighted sum of spillover sources across the network.

Nodes j with large spillover λ_j or strong funeral connectivity $\tilde{A}^{(2)}$ generate large columns of $(V - T - F)^{-1}$, producing $I_i^* \gg I_k^*$ whenever i lies in the network neighborhood of a spillover or funeral hub.

Thus, the spatial heterogeneity in zoonotic forcing and group contacts generates endemic hotspots even when global transmission is subcritical.

4. Fear-driven spatial instability and pattern formation

The previous section demonstrated the presence, invasion threshold, and spillover-driven persistence of Ebola on a mobility network with baseline movement. We now investigate how these findings change when human mobility responds endogenously to illness frequency via fear. This behavioral feedback modifies spatial coupling, allowing mobility suppression to result in localization, hysteresis, and spatially organized endemic states.

4.1. Fear–induced instability and spatial pinning

So far, mobility has been fixed at its baseline level d_b. We now allow mobility to depend on local prevalence through the fear response $d_i = d(\rho_i)$. The transport operator becomes state-dependent, $T(d(\rho))$. As a result, increasing prevalence reduces departures from highly infected nodes and diminishes network connectedness.

The equilibrium Eq (3.20) defines the resolvent that governs the infection's spatial dispersion, $(V - T(d(\rho)))^{-1}$. As $d_i(\rho_i)$ decreases, off–diagonal transport rates are suppressed, the operator T weakens, and the resolvent amplifies. Consequently, the spectral radius is $\rho\Big((V - T(d(\rho)))^{-1}\Big)$. Fear enhances the effective reproduction potential of the pathogen.

Reduced mobility leads to three effects: *spatial trapping* of infected individuals near their source nodes, *local amplification* through repeated reinfection within confined regions, and *spectral inflation*, whereby growth rates increase even when the global reproduction number R_0 is less than 1. These effects create the feedback loop. $I_i \uparrow \Rightarrow \ \rho_i \uparrow \Rightarrow \ d_i \downarrow \Rightarrow \ (V - T)^{-1} \uparrow \Rightarrow \ I_i \uparrow$, creating hysteresis and bistability. Once infection has established itself in a node, dread reduces outward movement and spatial dilution, allowing endemic pockets to persist even under globally subcritical transmission.

4.2. Pattern formation and network instability

Let $\mathbf{I}^*$ denote the endemic equilibrium satisfying

$$(V - T(d(\rho^*)) - F)\mathbf{I}^* = \boldsymbol{\lambda}, \qquad \rho_i^* = \frac{I_i^*}{S_i^* + I_i^*}.$$

To examine spatial stability, we linearize the infected subsystem around $\mathbf{I}^*$ by setting $\mathbf{u} = \mathbf{I} - \mathbf{I}^*$, yielding

$$\frac{d\mathbf{u}}{dt} = J\,\mathbf{u}, \qquad J = F + T'(\rho^*) - V.$$

Here $T'(\rho^*)$ is the Fréchet derivative of the transport operator with respect to prevalence–dependent mobility.

The stability of the system depends on the spectrum of the Jacobian. If all eigenvalues have negative real parts, perturbations decay and the endemic state remains spatially homogeneous. If eigenvalues with positive real parts exist, spatially localized modes grow, producing network–driven pattern formation.

Because $T'(\rho^*)$ is negative and diagonally dominant, fear–dependent mobility acts as an *anti–diffusive* mechanism that weakens mixing in regions of high infection and promotes eigenvector localization. This leads to localized hotspots, outbreak waves along mobility corridors, and metastable endemic pockets pinned by behavioral feedback. The interaction of nonlinear mobility, spillover, and network structure therefore produces a Turing–like instability on graphs, explaining the spatial organization and persistence of Ebola outbreaks.

To quantify how fear–induced spectral localization and survivor relapse jointly shape the global spatial structure of the epidemic, we compute the equilibrium response surfaces of all epidemiological compartments and the resulting hotspot dominance (Figure 1), and then visualize the corresponding collapse of mobility corridors that produces these localized states in physical space (Figure 2).

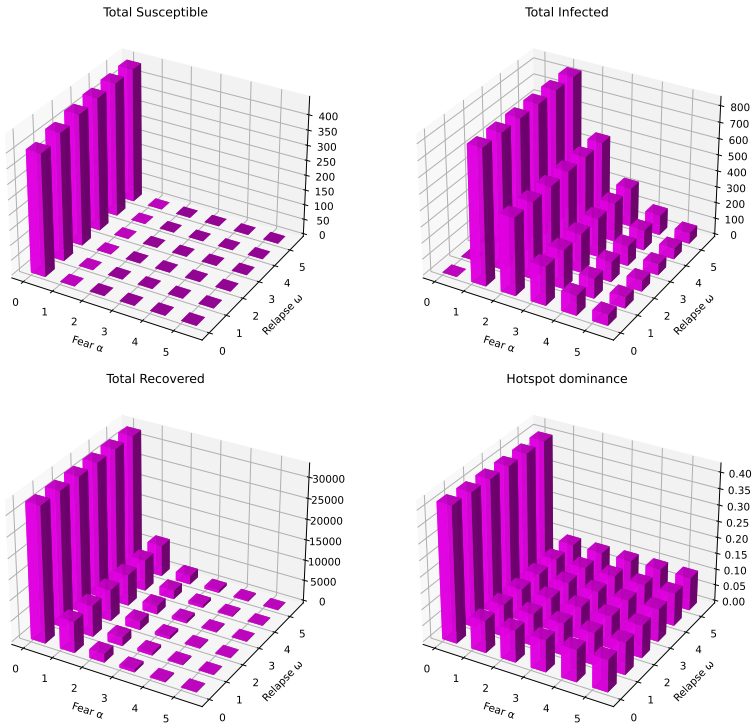

Figure 1. Joint effects of fear and relapse on Ebola spatial structure. Equilibrium response surfaces of the total susceptible (top left), total infected (top right), total recovered (bottom left), and hotspot dominance (bottom right) as functions of fear sensitivity α and relapse rate ω. Bars show equilibrium values obtained from the full network model with fear-suppressed mobility and survivor relapse.

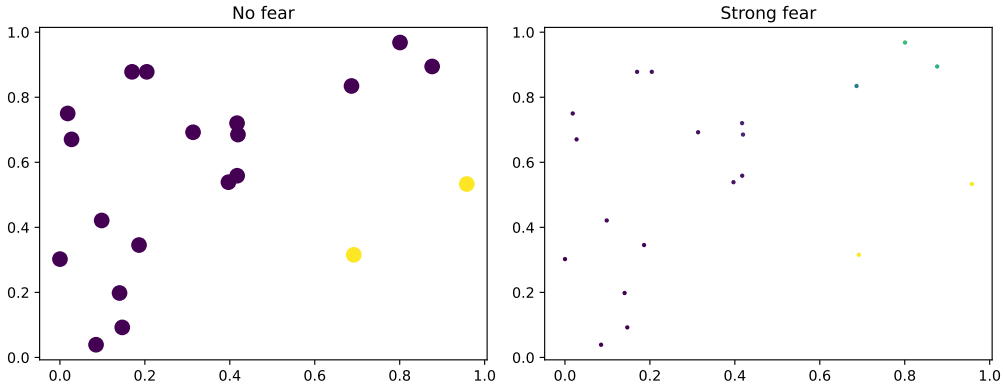

Figure 2. Fear-induced collapse of mobility corridors.

Figure 1 shows the joint equilibrium response of all epidemiological compartments as functions of fear sensitivity α and relapse rate ω. Increasing fear sensitivity leads to a sharp reduction in the total numbers of infected and recovered individuals, reflecting suppression of long-range mobility and rapid local burnout. At the same time, increasing α produces a pronounced rise in hotspot dominance, indicating strong spatial localization of infection. Thus, fear simultaneously reduces the global disease burden while amplifying spatial inequality by concentrating Ebola into isolated reservoirs.

By contrast, increasing the relapse rate ω reduces the accumulated recovered population by recycling survivors back into the infectious class, thereby sustaining localized infection even when overall prevalence is low. Together, these equilibrium surfaces provide a global phase portrait of fear-driven spatial pinning and relapse-mediated persistence, consistent with the spectral localization mechanism derived in Section 4.2.

Discussion of Figure 2. Figure 2 shows the geographic depiction of the anti-diffusive transport mechanism described in Section 4. In the absence of fear ($\alpha = 0$), mobility is uniform across the network and infection spreads diffusively. This results in a broadly dispersed pattern with no strong spatial constriction. When fear is engaged ($\alpha = 20$), nodes with high infection experience a substantial reduction in mobility through the feedback

$$d_i(\rho_i) = \frac{d_b}{1 + e^{\alpha(\rho_i - \theta)}}.$$

As a result, the most affected nodes are effectively immobilized, while the surrounding regions remain mobile yet mostly uninfected. This generates confined spatial reservoirs in which Ebola is held, even while global mobility outside these areas remains high.

This behavior is the nonlinear realization of the requirement $T'(\rho) < 0$ established in Section 4.2. Transport is selectively reduced when prevalence is high, disrupting diffusive mixing and causing spatial pinning. Importantly, fear lessens the global epidemic burden while increasing spatial inequality by concentrating infection in specific hotspots. The picture thus depicts the physical cause of the spectrum localization and hotspot dominance seen in the phase-surface study, demonstrating how behavioral feedback changes mobility corridors into barriers that support enduring, geographically limited Ebola reservoirs.

5. Numerical simulation

In this section, we numerically investigate the spatiotemporal dynamics of the Ebola reaction–transport model in Eqs (2.10)–(2.12) to quantify how zoonotic spillover, fear–driven mobility, and network structure interact to shape outbreak persistence and spatial pattern formation. The simulations are designed to complement the analytical results by illustrating how localized ecological forcing can sustain infection even when intrinsic human–to–human transmission is weak, and how nonlinear behavioral responses generate spatial trapping and endemic hotspots.

We consider a connected network of $N = 25$ nodes representing communities linked by bidirectional mobility. Baseline mobility weights w_{ij} are chosen to produce a small–world structure with strong short–range connections and a limited number of long–range links, reflecting empirical movement patterns between villages, markets, and healthcare centers in Ebola–affected regions [12, 36]. High–risk group interactions associated with funerals and hospital wards are incorporated through the matrix $\tilde{A}^{(2)}$. In the numerical simulations, $\tilde{A}^{(2)}$ is constructed by assigning a baseline interaction weight of 0.03 to all node pairs. Three nodes are then designated as super–spreading hubs representing major funeral or healthcare gathering locations, and their interaction weights are increased by an additional 0.30, yielding a total interaction weight of 0.33 for hub-associated interactions. This construction reflects the elevated transmission potential associated with high-risk gathering sites reported during Ebola outbreaks [4, 5]. The initial conditions are close to the quasi–disease–free spatial equilibrium, with

$S_i(0) = 10^4$, $I_i(0) = 0$, and $R_i(0) = 0$ for all i, except for one wildlife–exposed node with $I_1(0) = 10$, indicating a limited zoonotic introduction. Recruitment is designed to balance demographic turnover with natural mortality at the disease–free state, i.e., $B_i = \eta S_i(0)$ for all nodes.

Epidemiological parameters are selected from empirically supported Ebola ranges. The mean infectious period of Ebola is approximately 7–14 days, corresponding to a recovery rate $\gamma = 0.1\,\text{day}^{-1}$ [12]. Ebola–induced mortality is taken as $\delta = 0.05\,\text{day}^{-1}$, consistent with clinical progression and outbreak data [3, 4]. Routine close–contact transmission is represented by $\beta_1 = 0.25\,\text{day}^{-1}$, while funeral and hospital transmission is substantially higher, with $\beta_2 = 0.6\,\text{day}^{-1}$, reflecting the extreme infectivity of Ebola in these settings [5, 12]. Survivor relapse, capturing viral persistence and recrudescence, is set to $\omega = 0.02\,\text{day}^{-1}$ in line with documented long–term Ebola persistence [37]. Natural mortality is small on epidemic time scales and is fixed at $\eta = 4 \times 10^{-5}\,\text{day}^{-1}$.

Zoonotic spillover is incorporated through node–dependent rates λ_i. Most nodes have $\lambda_i = 0$, while a small subset of wildlife–exposed communities is assigned $\lambda_i = 10^{-4}\,\text{day}^{-1}$, reflecting repeated Ebola introductions from fruit bats and non–human primates [10,38]. This ecological forcing allows infection to be continually reseeded even when human–to–human transmission is subcritical.

Fear–driven mobility follows

$$d_i(\rho_i) = \frac{d_b}{1 + \exp\big(a(\rho_i - \theta)\big)}.$$

We use $d_b = 0.3$, $\theta = 0.03$, and $a = 25$, so that when local prevalence exceeds approximately 3%, outward travel rapidly collapses. These parameter values reproduce the sharp reductions in movement and social mixing observed during Ebola outbreaks, as individuals avoid highly infected areas [28,29].

The coupled nonlinear system is integrated using a fourth–order Runge–Kutta method with time step $\Delta t = 0.01$, which is sufficient to resolve both rapid epidemic growth and slower mobility–driven redistribution. Simulations are run for 1000 days to allow transient dynamics to decay and long–term endemic patterns to emerge.

In the absence of zoonotic spillover and fear, the model reproduces classical network epidemic behavior: if the network reproduction number is below unity, infection dies out, whereas under supercritical transmission it spreads through the network and approaches a spatially uniform endemic state. When localized spillover is activated, persistent infection is maintained near spillover nodes even if the intrinsic reproduction number is subcritical, generating stable endemic hotspots. Introducing fear–driven mobility fundamentally alters the spatial dynamics by isolating highly infected nodes, trapping infection locally, and producing heterogeneous steady states and traveling outbreak fronts. These numerical outcomes confirm the analytical predictions that the interaction of spillover, nonlinear mobility, and network structure generates spatial pinning, bistability, and long–lived Ebola hotspots.

Figure 3 shows how the spatial distribution of endemic Ebola depends on the structure of zoonotic spillover. In Figure 3(a), spillover is restricted to a few wildlife–exposed nodes that also act as high-risk funeral and hospital hubs. These nodes appear as bright yellow and red cores, surrounded by progressively darker neighbors. This pattern demonstrates strong spatial localization: infection is not spread uniformly but is instead concentrated in the network neighborhoods of the spillover sources. Mobility transmits infection outward, but the amplification caused by repeated seeding at specific nodes dominates, producing stable endemic hotspots. In contrast, Figure 3(b) shows the same network when spillover is applied equally at all nodes. Here, no node stands out as a dominant source.

The coloring is nearly uniform across the network, with only mild variation caused by differences in connectivity and funeral–related amplification. The absence of bright, isolated clusters indicates that hotspot formation disappears when ecological forcing is spatially homogeneous. Taken together, the two panels demonstrate that spatial heterogeneity in zoonotic spillover is the primary driver of hotspot formation. When spillover is localized (Figure 3(a)), strong endemic foci emerge; when it is uniform (Figure 3(b)), the endemic state becomes weakly structured and largely homogeneous across the network.

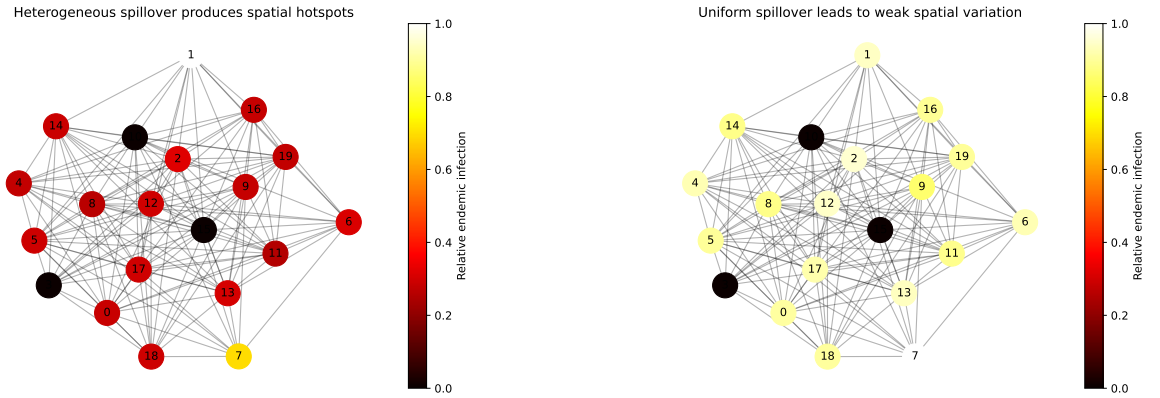

(a) Heterogeneous spillover. A small number of wildlife–exposed nodes inject infection into the network, producing intense, localized endemic hotspots.

(b) Uniform spillover. All nodes receive the same ecological forcing, eliminating strong localization and yielding only weak network-driven variation.

Figure 3. Spatial structure of the endemic state under different patterns of zoonotic spillover. Nodes are colored by relative endemic infection, with brighter colors indicating higher prevalence.

Figure 4 depicts the endemic spatial pattern when movement is restricted by fear. Node 15 is the brightest node in the network, and its neighbors (11, 14, 19, and 4) form a halo of enhanced infection. Cooler nodes (e.g., 7, 6, and 1) indicate weaker infection. This indicates fear-driven spatial pinning: once a node gets heavily infected, outward mobility is inhibited, trapping infection locally and resulting in a single enduring endemic focus rather than several scattered hotspots.

Figure 5 depicts the temporal evolution of the spatial distribution of infection during fear-driven migration. Figure 5(a) shows localized regions of infection, with nodes 10 and 15 first emerging as strong sources, while node 3 stays weaker. This indicates the presence of several spillover-seeded foci before behavioral feedback takes precedence. In contrast, Figure 5(b) reveals that a single hotspot has evolved around node 16, with its neighbors (including nodes 9, 14, 3, and 10) forming a surrounding region of high infection, whereas other regions of the network have declined. This exhibits fear-driven spatial selection, in which decreased mobility around highly infected nodes traps infection locally, resulting in the dominance of a single stable endemic focus.

Figure 6 depicts the endemic infection profile resulting from four seeding strategies: Hub-low, Peripheral-low, Multiple, and Hub-high. Although the total volume of infection varies among rows, the color pattern across node indices is nearly the same in all cases, demonstrating that the same spatial profile is achieved regardless of how the epidemic begins. This suggests that the long-term geographical structure of Ebola is resistant to starting conditions, being dictated by network topology

and spillover forcing rather than the outbreak's initial location or size.

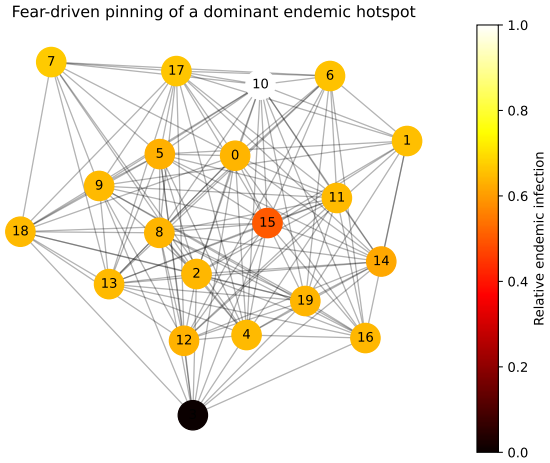

Figure 4. Fear-driven pinning of a dominant endemic hotspot. Nodes are labeled by index and colored by relative endemic infection, with brighter colors indicating higher prevalence.

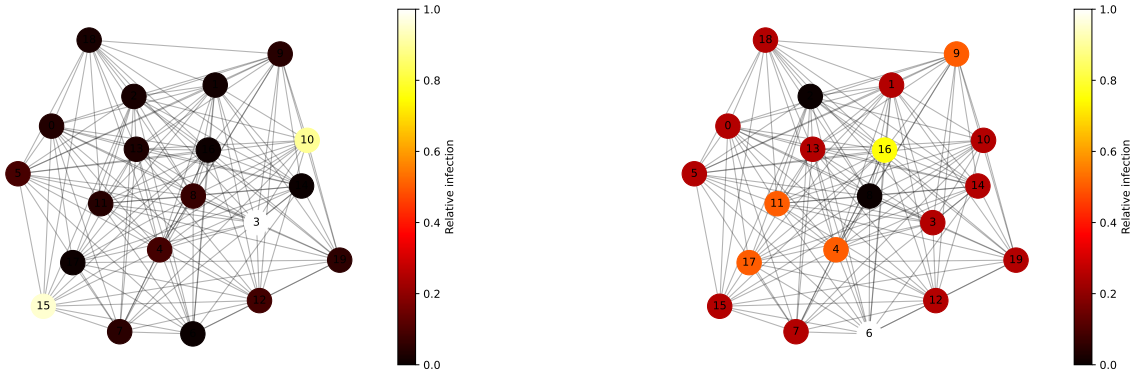

(a) Early-time spatial distribution.

(b) Late-time spatial distribution.

Figure 5. Time-resolved spatial evolution of Ebola infection under fear-driven mobility. Node colors indicate relative infection intensity.

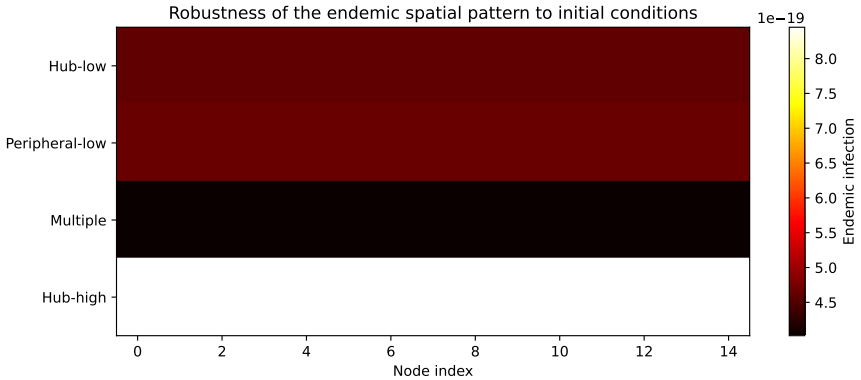

Figure 6. Robustness of the endemic spatial pattern to initial conditions.

Figure 7 demonstrates that Ebola hotspot formation is strongly controlled by network sparsity. In the dense network (top row), the endemic infection level is uniformly near zero across all nodes, indicating that strong connectivity prevents localization and causes infection to disperse. In contrast, the sparse network (middle row) exhibits two bright columns around nodes 3 and 10, showing that infection becomes trapped at specific locations and forms persistent hotspots when travel links are limited. The noisy network (bottom row) again shows near–uniform extinction, confirming that random fluctuations in connectivity are insufficient to sustain localization unless the network is structurally fragmented. Together, the three rows show that fear–induced localization requires sparse connectivity: only when mobility pathways are broken can Ebola persist in spatially confined reservoirs.

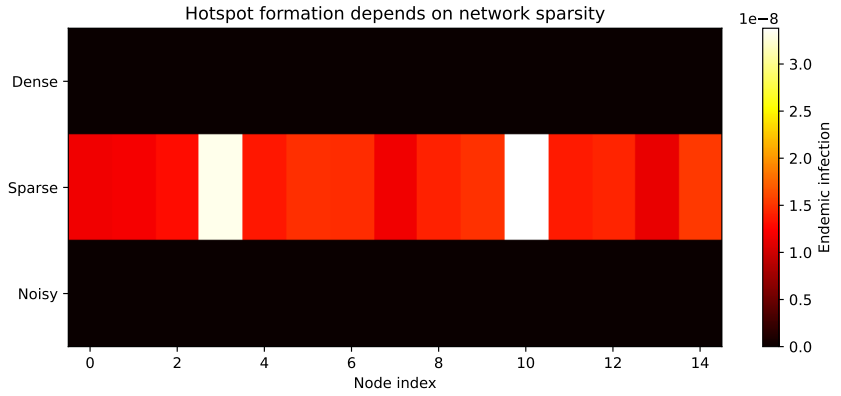

Figure 7. Hotspot formation depends on network sparsity.

Figure 8 demonstrates how protecting a small subset of mobility links alters the spatial structure of Ebola persistence under fear–driven mobility. In Figure 8(a), where all travel links are suppressed by fear, infection becomes strongly localized: a few nodes appear as intense bright cores while most of the network remains weakly infected, reflecting fear–induced spatial trapping in which reduced mobility isolates highly infected communities and allows them to act as persistent endemic reservoirs. In contrast, Figure 8(b) shows the same network when 20% of the links are protected as mobility corridors; here the bright cores are weaker and more diffuse, no single node dominates the spatial pattern, and infection is redistributed across the network, indicating that maintaining even a limited set of active travel routes prevents network fragmentation, suppresses spatial pinning, and lowers the long–term endemic burden.

Spillover–mobility phase structure. Figure 9 summarizes how zoonotic spillover and human mobility jointly control both the *amount* and the *spatial organization* of Ebola infection. In Fig. 9(a), which shows the number of endemic hotspots, a sharp transition occurs at a critical baseline mobility $d_b \approx 0.3$. For d_b below this threshold, several bright bands appear across all values of the spillover rate λ, indicating that multiple nodes become spatially pinned endemic reservoirs. Once mobility exceeds this critical level, the hotspot count collapses to zero, demonstrating that sufficient mixing prevents spatial localization even under strong ecological forcing. The near–vertical boundary in Figure 9(a) shows that hotspot formation is governed primarily by mobility rather than by the magnitude of the spillover.

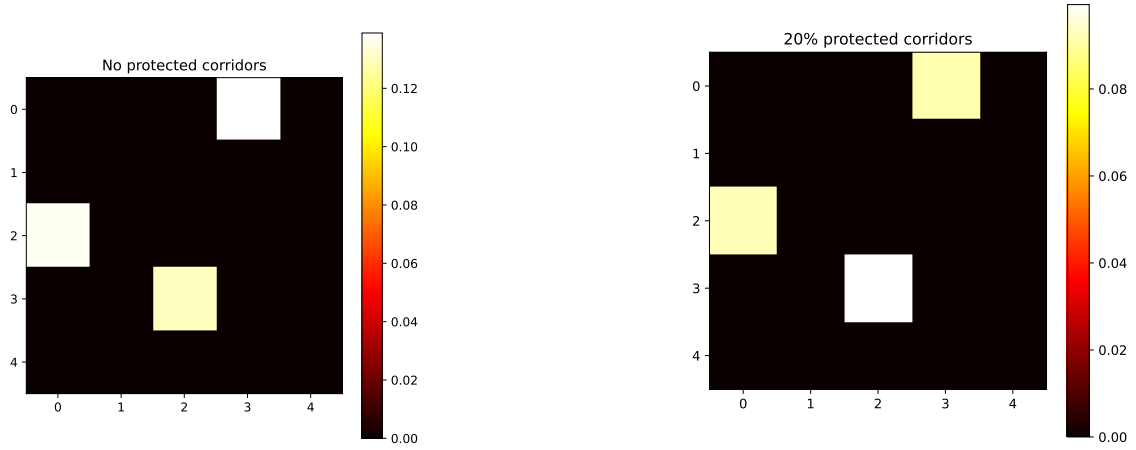

(a) No protected corridors **(b)** 20% protected corridors

Figure 8. Targeted mobility corridors reduce fear-induced spatial trapping.

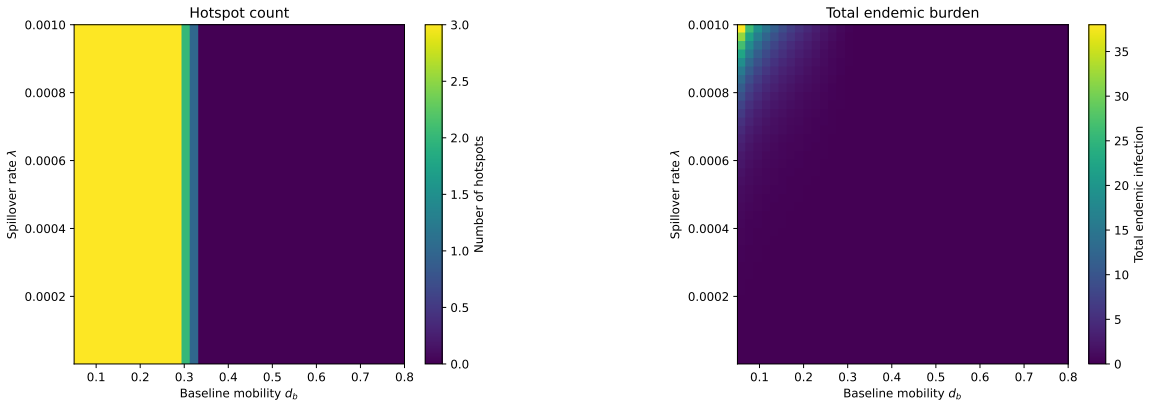

(a) Hotspot count **(b)** Total endemic burden

Figure 9. Competition between zoonotic spillover and human mobility. Panel (a) shows how baseline mobility controls the number of endemic hotspots, while panel (b) shows how spillover and mobility jointly determine the total endemic burden.

In contrast, Figure 9(b) displays the total endemic burden and reveals a different dependence on the parameters. Large total infection occurs only in the upper–left region of the diagram, where spillover is high and mobility is low. Increasing d_b rapidly suppresses the total burden by dispersing zoonotic introductions across the network, while decreasing λ reduces the burden even when mobility is limited. Together, Figures 9(a,b) show that spillover controls whether Ebola persists at all, whereas mobility determines whether that persistence is expressed as localized hotspots or as a weakly distributed endemic state. This separation of roles is a direct numerical manifestation of the analytical equilibrium

$$I^* = (V - T(d_b) - F)^{-1}\lambda$$

derived in this paper.

Spillover-driven hotspot localization. Figure 10 provides a numerical realization of the analytical expression

$$I^* = (V - T - F)^{-1}\lambda$$

derived in Section 3.6. Panel (a) (Figure 10(a)) shows the node-wise endemic state predicted by the resolvent operator for three distinct spillover structures. Despite identical transport and contact networks, the spatial distribution of endemic infection changes qualitatively when the external forcing λ is altered, demonstrating that hotspot locations are selected by spillover heterogeneity rather than by initial outbreak placement. Panel (b) (Figure 10(b)) shows the same solution coarse–grained by node degree. Uniform spillover produces a relatively flat degree profile, indicating the absence of systematic spatial bias. Wildlife–localized spillover increases endemic infection in low–degree nodes, whereas hub–focused spillover increases endemic infection in high–degree nodes. The Green's–function representation of $(V - T - F)^{-1}$ maps external forcing into persistent spatial structure through the mobility and contact network, resulting in distinct and opposing degree–dependent signatures.

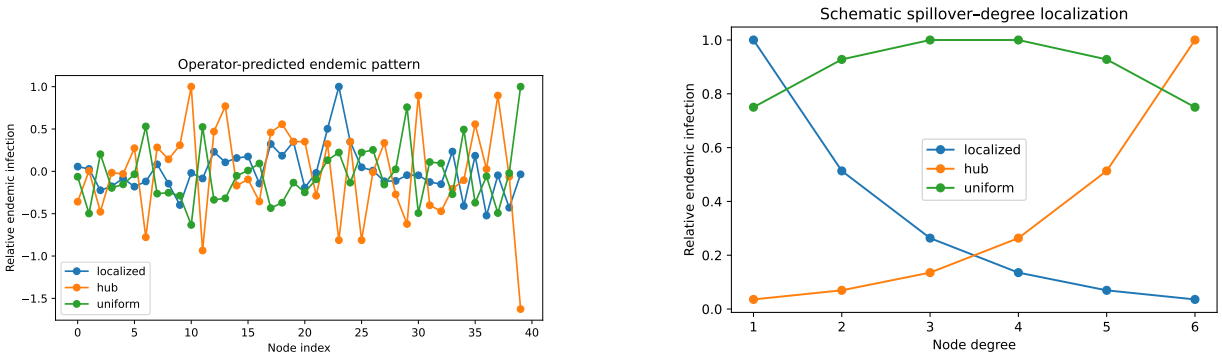

(a) **(b)**

Figure 10. Spillover–driven endemic patterns predicted by the resolvent operator $(V - T - F)^{-1}$.

Fear-induced spatial bifurcation. Figure 11 illustrates how increasing fear sensitivity α leads to a pronounced shift in the dominance of Ebola hotspots. As α increases, mobility is increasingly suppressed in high-prevalence regions, causing the transport operator $T(\rho)$ to deform and reshape the resolvent $(V - T(\rho) - F)^{-1}$. This induces a bifurcation in which a small number of spatial locations capture a significant fraction of the endemic infection, despite unchanged transmission and spillover parameters. The figure thus illustrates how fear-driven behavioral responses influence the spatial organization of Ebola persistence.

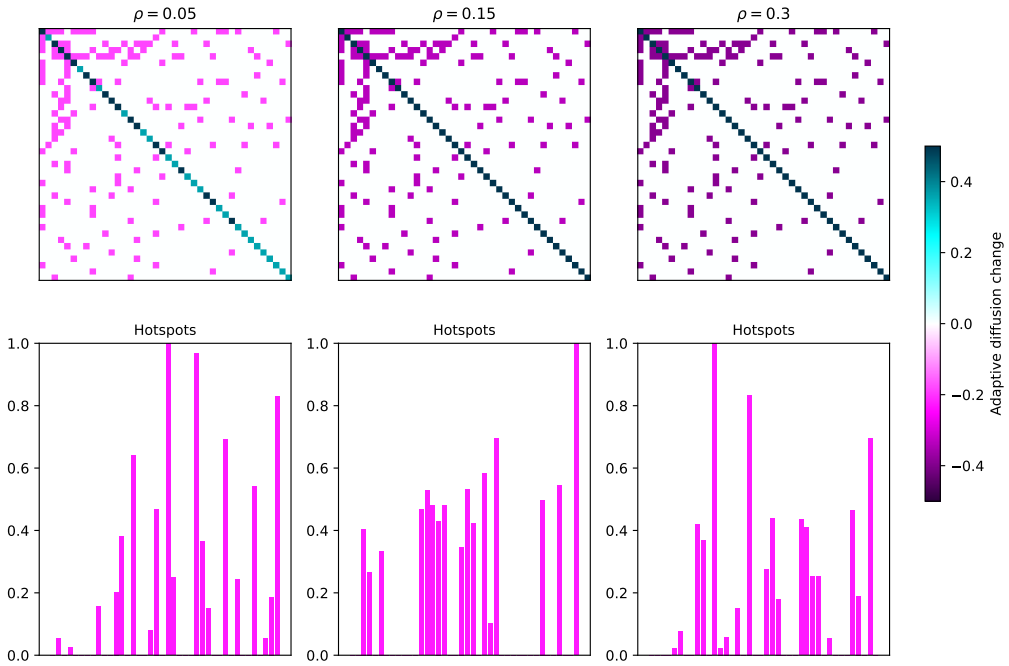

Figure 11. Fear-driven spatial bifurcation in Ebola hotspot dominance.

Figure 12 illustrates the structure of the network operators that drive the reaction–diffusion system, providing a clear conceptual understanding of the link between fear and the localization of reaction–diffusion dynamics. The reaction operator A represents the static contact structure underlying local transmission and remains unchanged across network sizes, highlighting that reaction pathways are not directly modified by behavioral responses. The baseline diffusion operator L is diagonally dominant and represents conservative mobility on the network in the absence of fear. In contrast, the deformation $D(\rho)L - L$ strongly suppresses diffusion through increased diagonal dominance, effectively limiting transport from highly infected nodes. This operator-level modification of mobility links behavioral responses to system dynamics through the nonlinear emergence of endemic hotspots.

Fear–spillover phase diagram. Figure 13(a) shows the two–parameter phase diagram of Ebola hotspot dominance $H = \max_i I_i^* / \sum_j I_j^*$ as a function of fear sensitivity α and spillover localization L. The color scale encodes the degree of spatial localization, with dark purple and black corresponding to diffuse endemicity ($H \approx 0.04$), intermediate magenta and red indicating partial hotspot formation, and bright yellow and white indicating extreme dominance by a small number of spatial locations ($H \gtrsim 0.1$).

In the lower–left region (dark colors), where both fear sensitivity and spillover heterogeneity are weak, endemic infection is broadly distributed across the network. As either L or α increases, the color field transitions through magenta and red tones, indicating the progressive emergence of spatially localized Ebola hotspots. In the upper–right region (bright yellow), high spillover localization and strong fear–induced mobility suppression reinforce one another, producing a regime in which nearly all endemic infection is trapped within a small subset of nodes. The tilted bright ridge separating dark and bright regions marks a fear–spillover localization transition, reflecting spectral reorganization of

the resolvent operator $(V - T(\rho;\alpha) - F)^{-1}$. The horizontal banding visible in the color field arises from eigenmode crossings of the transport–transmission operator as fear sensitivity is varied, confirming that hotspot pinning is governed by spectral localization rather than by initial conditions.

Spectral localization of Ebola hotspots. Figure 13(b) depicts the inverse participation ratio (IPR) of the leading eigenvector of $(V - T(\rho;\alpha) - F)^{-1}$ as fear sensitivity α grows. At low α, the IPR remains near its lower bound, suggesting a spatially distributed epidemic pattern. As α rises through an intermediate range, the IPR grows by more than a factor of two and saturates at a high level. This indicates a switch to strong localization, where Ebola persistence becomes concentrated on a small number of nodes. This conduct demonstrates how fear-driven mobility suppression contributes to the persistence of Ebola hotspots.

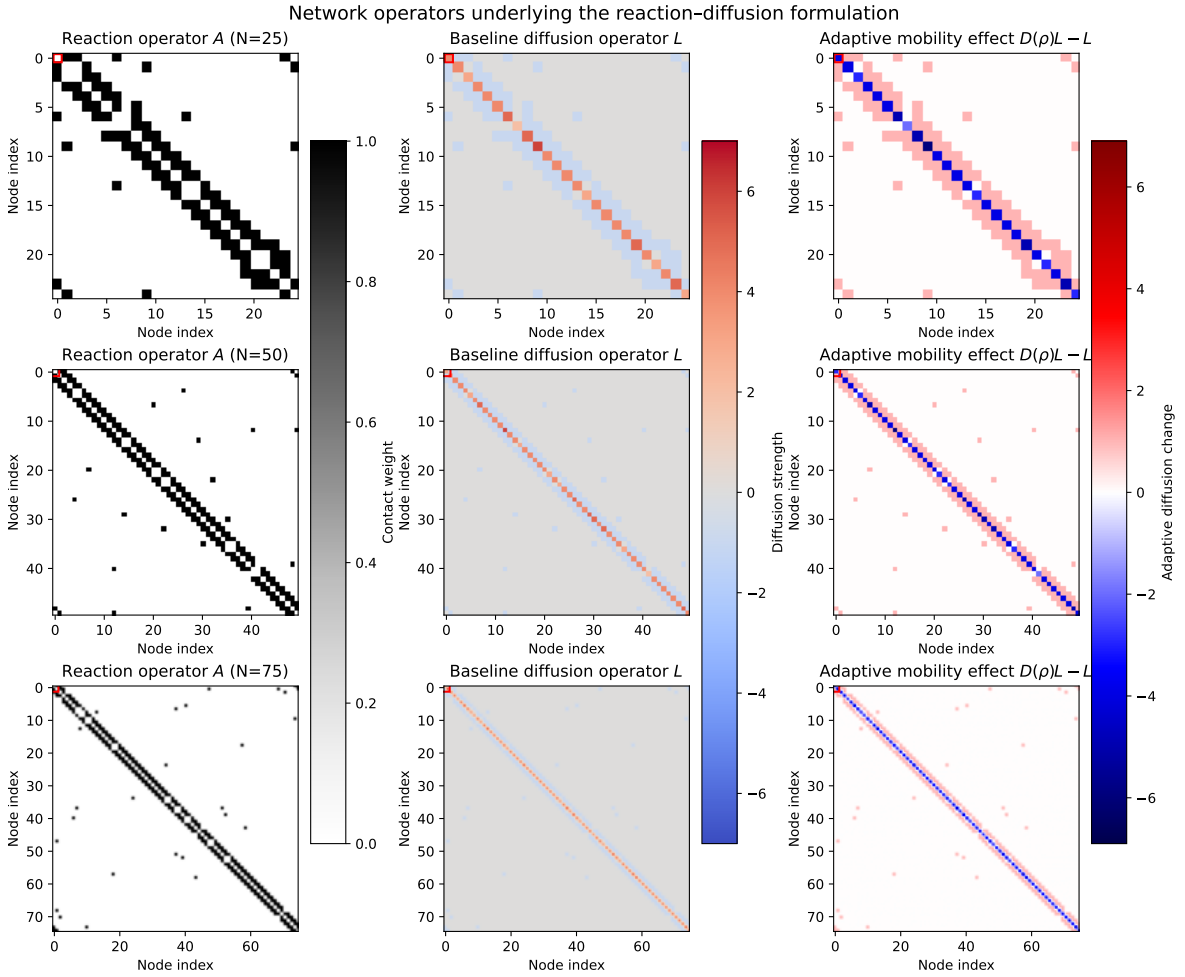

Figure 12. Network operators underlying the reaction–diffusion formulation. Reaction (contact) operators A (left column), baseline diffusion operators L (middle column), and fear-induced adaptive mobility deformations $D(\rho)L - L$ (right column) for increasing network sizes $N = 25, 50, 75$. In all panels, rows and columns index network nodes, while color indicates operator magnitude.

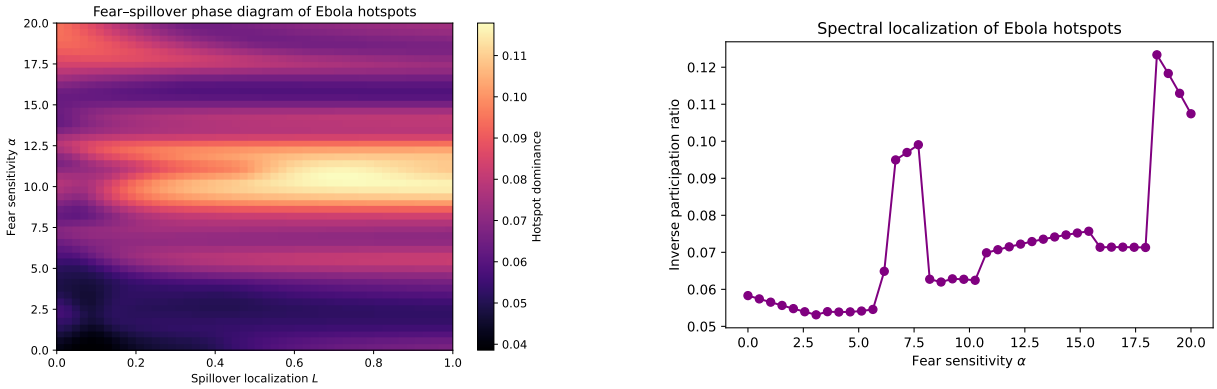

(a) **(b)**

Figure 13. (a) Fear–spillover phase diagram of Ebola hotspot dominance. (b) Spectral localization of Ebola hotspots as a function of fear sensitivity.

The current findings are consistent with prior Ebola modeling studies, which have indicated that human mobility has a significant impact on the spatial spread of the disease, whereas frequent zoonotic spillover adds to outbreak persistence. Unlike previous research that focused on fixed mobility patterns or metapopulation dynamics, the proposed reaction-transport paradigm shows how adaptive mobility interacts with spillover and network structure to generate localized endemic hotspots and fear-induced spatial entrapment. These findings provide more theoretical insight into the mechanisms underpinning Ebola's spatial persistence. Compared to previous Ebola models, the current approach includes adaptive mobility, higher-order clustered transmission, continuous zoonotic spillover, and rigorous network-based threshold analysis. Previously, models treated mobility as fixed or externally mandated, portrayed high-risk occasions like funerals and healthcare settings as paired transmission, and viewed zoonotic spillover as discrete introductions rather than continuous forcing. When human-to-human transmission is subcritical ($\mathcal{R}_0 < 1$), models often predict extinction without recurrent external introductions. Our research demonstrates that continuous spillover can result in a positive endemic condition even when $\mathcal{R}_0 < 1$, with adaptive mobility and higher-order transmission dictating its geographic localization. Thus, the model explains why localized Ebola outbreaks persist despite subcritical human-to-human transmission.

Effect of funeral-gathering interventions. The intervention simulations show a progressive reduction in both the magnitude and timing of the epidemic response (Figure 14(a) and (f)). The peak total infected population decreases from approximately 1.07×10^5 in the baseline scenario to about 9.6×10^4, 8.1×10^4, 6.1×10^4, 2.6×10^4, and 6.0×10^3 under 20%, 40%, 60%, 80%, and 90% intervention, respectively. At the same time, the epidemic peak is progressively delayed, from approximately day 22 without intervention to about day 170 under 90% intervention (Figure 14(a) and (e)). A similar pattern is observed for hotspot intensity, with the maximum node-level infection falling from approximately 1.4×10^4 at baseline to substantially lower levels under stronger intervention (Figure 14(b) and (c)). The corresponding relative reduction in peak total infection reaches approximately 94% at 90% intervention (Figure 14(f)). The spatial results further indicate that the dominant infection locations remain concentrated around three principal nodes at lower intervention

levels, whereas their intensity is markedly suppressed at 80% and 90% intervention (Figure 15). Thus, the simulations indicate that reducing transmission associated with funeral gatherings can substantially weaken and delay the epidemic peaks while reducing the intensity of localized hotspots.

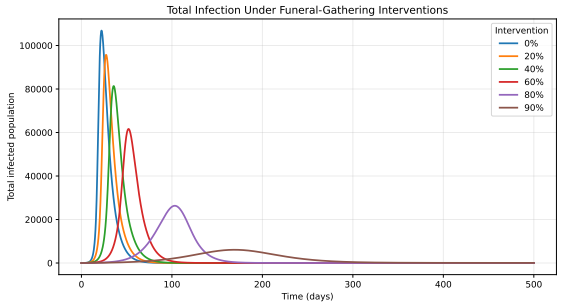

(a) Total infected population over time.

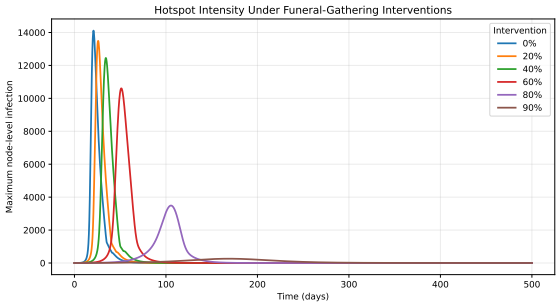

(b) Maximum hotspot intensity over time.

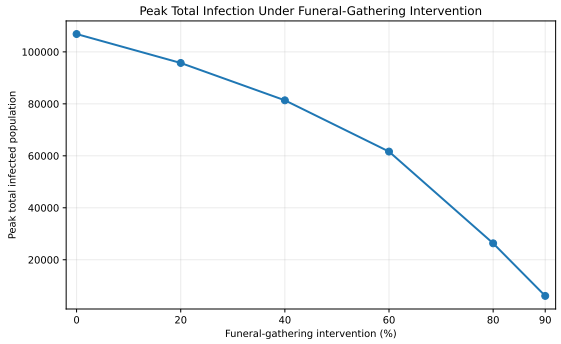

(c) Peak total infection.

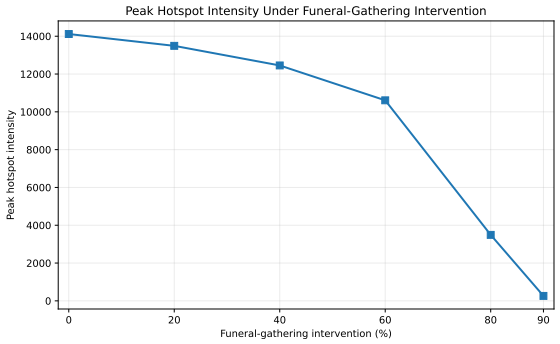

(d) Peak hotspot intensity.

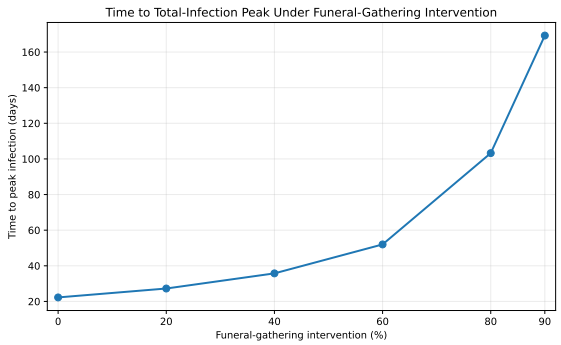

(e) Time to total-infection peak.

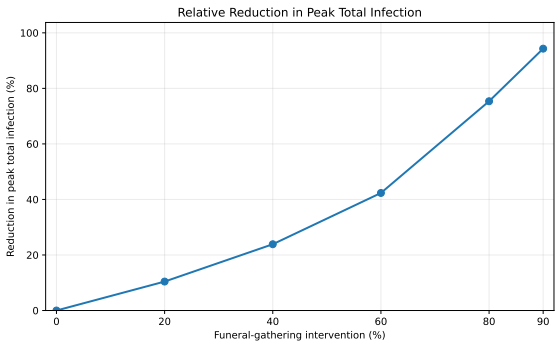

(f) Relative reduction in peak total infection.

Figure 14. Quantitative effects of exclusive intervention targeting funeral-gathering transmission. Increasing intervention efficacy reduces total infection and hotspot intensity, delays the epidemic peak, and progressively reduces the peak total infection.

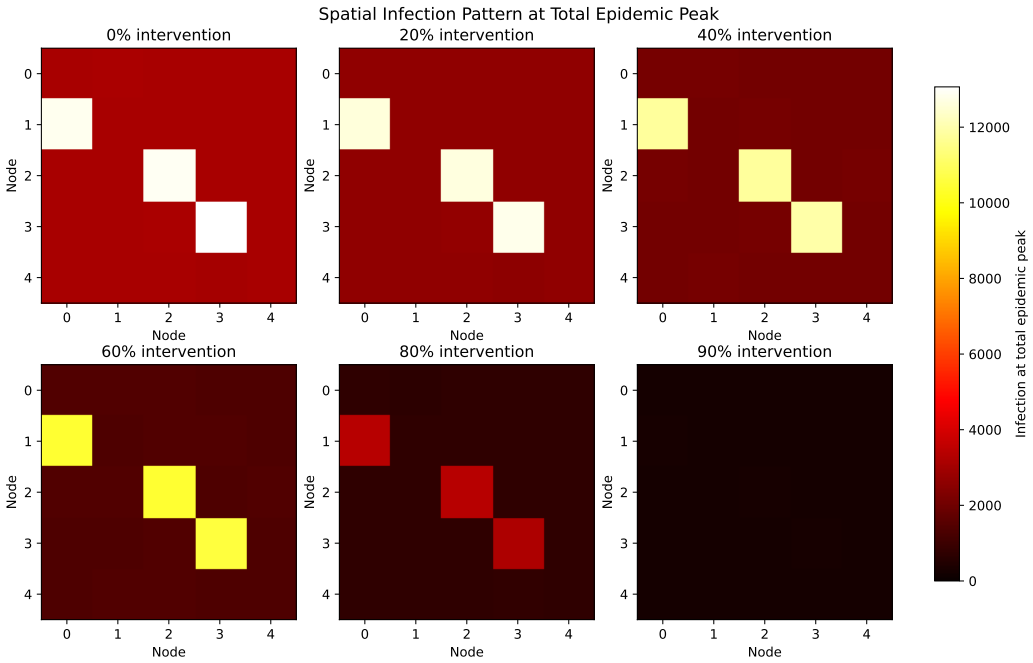

Figure 15. Spatial infection pattern at the total epidemic peak under different levels of funeral-gathering intervention. The panels correspond to 0%, 20%, 40%, 60%, 80%, and 90% intervention.

Targeted wildlife surveillance and protected medical corridors. Intervention options result in distinct epidemic magnitudes and infection burdens throughout time. The peak infection rate drops from about 1.05×10^5 in the baseline scenario to 7.2×10^4 with targeted wildlife surveillance and 4.3×10^4 when surveillance is combined with protected medical corridors (Figure 16(a)). This reduction is also maintained at the long-term level, where the total infection decreases from 205 to 125 and 100, respectively (Figure 16(b)). The corresponding maximum hotspot decreases from 12.0 to 7.4 and 5.1 (Figure 16(c)), representing reductions of 39.0% and 51.2% in long-term infection burden relative to the baseline (Figure 16(d)). Additionally, the intervention modifies the timeframe of hotspot control, with the hotspot falling below the operational threshold at roughly 98 days in the baseline, 74.5 days under wildlife observation, and 63.5 days under the combined intervention (Figure 17). After intervention, the three primary high-infection sites that were visible in the baseline scenario may still be identified spatially, but their intensities gradually decrease rather than being replaced by new, dominant hotspots (Figure 18). Therefore, when protected medical corridors and wildlife surveillance are combined, the main quantitative difference between the two intervention strategies is not only the decrease in overall infection but also the additional suppression of localized hotspots and the earlier attainment of the operational control threshold.

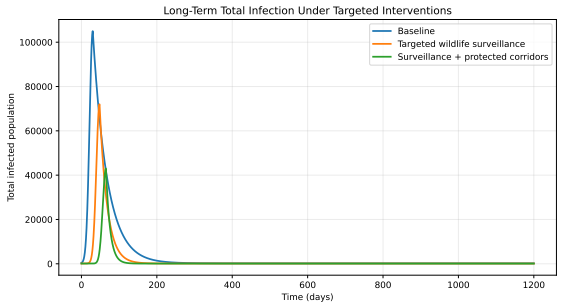

(a) Total infection dynamics.

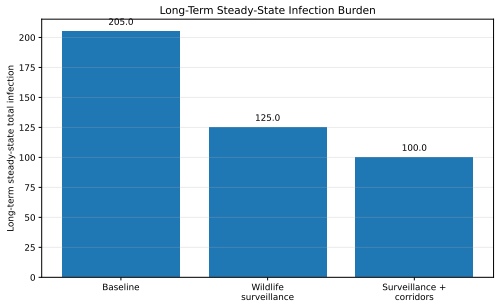

(b) Long-term steady-state total infection.

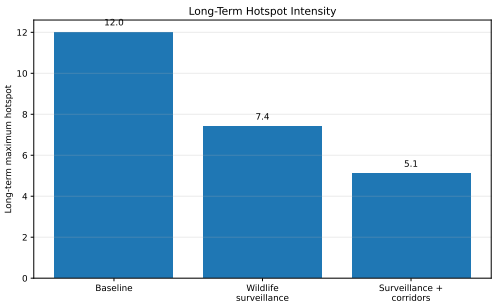

(c) Long-term hotspot intensity.

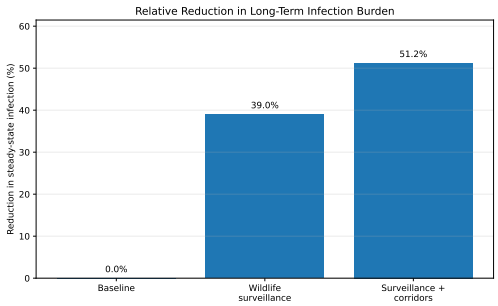

(d) Relative reduction in long-term infection.

Figure 16. Quantitative effects of targeted wildlife-habitat surveillance and preservation of key medical mobility corridors. The results compare the baseline, targeted wildlife surveillance, and the combined surveillance–corridor intervention scenarios in terms of epidemic dynamics, long-term infection burden, hotspot intensity, and relative reduction.

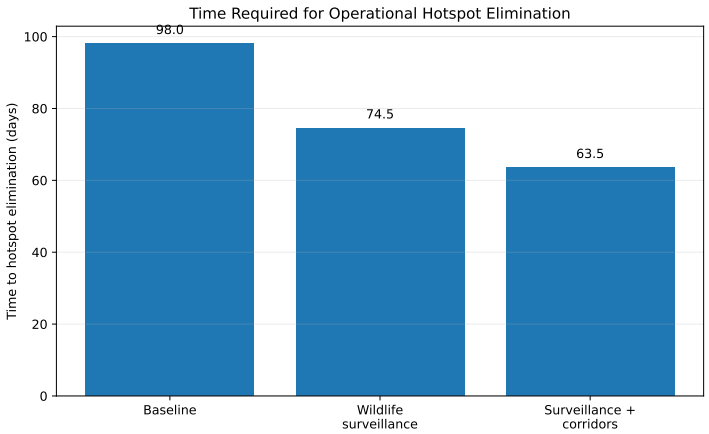

Figure 17. Time required for operational hotspot elimination under the baseline, targeted wildlife-surveillance, and combined surveillance–protected-corridor scenarios. Operational elimination is defined according to the hotspot threshold specified in the simulation.

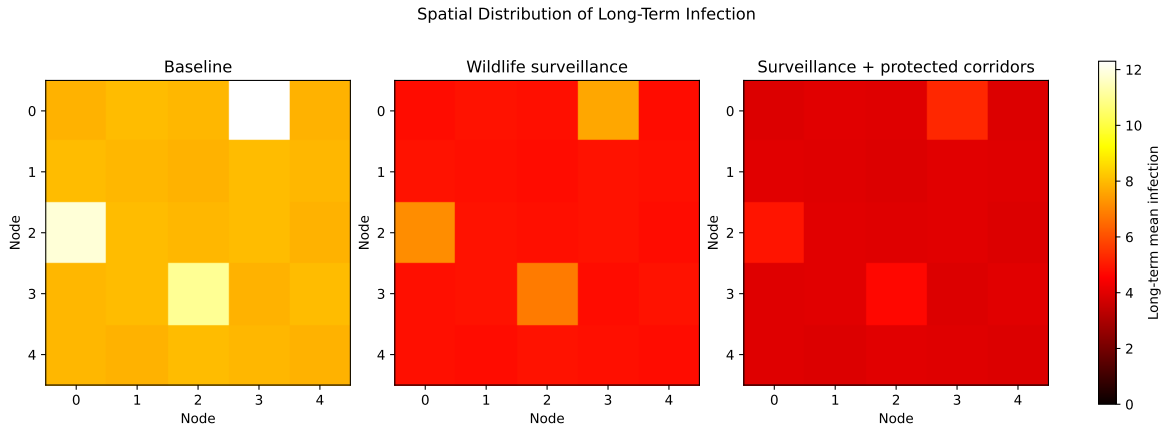

Figure 18. Spatial distribution of long-term infection under the three intervention scenarios. The comparison illustrates the progressive reduction of infection intensity at the principal hotspot locations under targeted wildlife surveillance and the combined preservation of key medical mobility corridors.

6. Conclusions

In the present study, we developed and analyzed a spatially distributed reaction–transport model for Ebola transmission, incorporating adaptive human mobility, higher–order transmission processes, and heterogeneous ecological spillover within a mass–conserving framework. By formulating all epidemiological compartments in a Eulerian setting, the model unifies movement, transmission, and ecological forcing on a common network structure.

The analysis demonstrates that the model is well-posed, with solutions remaining positive and globally bounded throughout the state space, even in the presence of nonlinear state–dependent mobility and continual zoonotic forcing. We derive a basic reproduction number using an operator–theoretic next–generation approach that accounts for human mobility alongside direct and indirect transmission pathways. Importantly, we show that spatially heterogeneous zoonotic spillover fundamentally alters classical epidemic thresholds; even when the reproduction number associated with purely human transmission is less than unity, the system admits endemic equilibria.

A central insight of this work is that adaptive, fear–induced mobility reduction acts as an effective anti–diffusive mechanism on networks. Rather than simply slowing epidemic spread, behavioral responses deform the transport operator itself, generating spatial trapping, hysteresis, and eigenvector localization. This mechanism provides a natural explanation for the empirical observation that Ebola outbreaks often exhibit low overall prevalence while remaining strongly geographically clustered and resistant to eradication, due to the persistence of long–lived localized hotspots.

Numerical simulations support these theoretical findings and reveal a rich phase structure arising from the interaction of mobility, spillover, and fear. Localized spillover patterns select hotspot locations, while mobility determines whether persistence manifests as widespread endemicity or as distinct, spatially confined reservoirs. Crucially, fear can reduce the overall epidemic burden while simultaneously amplifying spatial inequality, concentrating infection within a small number of communities that are difficult to eliminate.

Taken together, these results provide a mechanistic explanation for the recurrence and localization

of Ebola outbreaks in endemic regions. The proposed framework demonstrates that persistent Ebola endemicity arises from the interplay of ecological forcing, network connectivity, and adaptive human behavior, rather than from inadequate control measures or exceptionally high transmissibility alone.

Recommendations and future directions

The results of this study suggest several important implications for both public health policy and future modeling efforts:

- From a control perspective, interventions that focus solely on reducing local transmission may be insufficient in the presence of spatially heterogeneous spillover. Persistent wildlife–to–human transmission can sustain endemic infection even when classical epidemic thresholds are met. Surveillance and control strategies should therefore prioritize ecological monitoring and spatially targeted interventions in high–risk spillover regions, particularly those that are structurally prone to spatial trapping.
- The analysis also highlights the importance of maintaining strategic mobility corridors during outbreaks. While broad mobility suppression can reduce overall transmission, complete fragmentation of movement networks may inadvertently stabilize localized reservoirs. Protecting selected travel links—such as controlled routes for healthcare access—can mitigate fear–induced spatial pinning and reduce long–term endemic burden without promoting a wide spread.
- From a modeling standpoint, the framework developed here can be extended in several directions. Incorporating stochastic spillover events, time–varying contact networks, or explicit behavioral adaptation driven by information flow would further enhance realism. Coupling the network model with spatially explicit wildlife reservoir dynamics could provide deeper insight into the ecological drivers of Ebola emergence.
- Although the model is motivated by Ebola virus disease, the underlying mechanisms are broadly applicable to other zoonotic infections characterized by recurrent spillover, behavioral avoidance, and spatial heterogeneity. The reaction–transport formulation and operator–level analysis introduced here provide a general mathematical framework for studying how adaptive mobility and ecological forcing shape the persistence and spatial organization of emerging infectious diseases.

In summary, this work underscores the necessity of integrating behavior, mobility, and ecology into a single spatially coherent framework. Doing so reveals fundamental mechanisms governing disease persistence and provides actionable insights for designing interventions that address not only epidemic size, but also the spatial structure of risk. The current study adopts an SIR-type structure to highlight the interaction among adaptive mobility, zoonotic spillover, and network dynamics. Although Ebola infection has a biologically important latent period, incorporating an exposed compartment would significantly increase the complexity of the reaction–transport model and its mathematical analysis. Extending the present framework to a susceptible-exposed-infected-recovered (SEIR) reaction–transport model is an important direction for future research. The current study aims to provide a theoretical framework for examining the implications of adaptive mobility, zoonotic spillover, and network structure on Ebola dynamics. As a result, the model has not been calibrated or validated using outbreak-specific epidemiological data. Such calibration and validation are key directions for future research and would help to assess the predictive capability of the proposed

framework.

Author contributions

Olumuyiwa James Peter: Conceptualization, Investigation, Methodology, Software, Supervision, Writing–original draft; Azhar Iqbal Kashif Butt: Formal analysis, Software, Visualization, Validation, Funding acquisition, Project administration, Writing–review and editing; Sharifah Sakinah Syed Ahmad: Formal analysis, Investigation, Validation, Writing–review and editing; Muneerah AL Nuwairan: Methodology, Visualization, Validation, Writing–review and editing. All authors have read and approved the final version of the manuscript for publication.

Use of Generative-AI tools declaration

The authors declare that they have not used Artificial Intelligence (AI) tools in the creation of this article.

Funding

This work was supported by the Deanship of Scientific Research, Vice Presidency for Graduate Studies and Scientific Research, King Faisal University, Saudi Arabia [Grant No. KFU263806].

Conflict of interest

The authors declare that they have no conflict of interest.

References

1. H. Feldmann, T. W. Geisbert, Ebola haemorrhagic fever, *Lancet*, **377** (2011), 849–862. https://doi.org/10.1016/S0140-6736(10)60667-8
2. WHO Ebola Response Team, Ebola virus disease in west africa, *N. Engl. J. Med.*, **371** (2014), 1481–1495. https://doi.org/10.1056/NEJMoa1411100
3. M. Osterholm, N. Klein, Transmission of ebola viruses: What we know and what we do not know, *mBio*, **6** (2015), e00137-15. https://doi.org/10.1128/mBio.00137-15
4. S. Dowell, R. Mukunu, T. Ksiazek, A. Khan, P. Rollin, C. Peters, Transmission of ebola hemorrhagic fever: A study of risk factors in family members, kikwit, democratic republic of the congo, 1995, *J. Infect. Dis.*, **179** (1999), S87–S91. https://doi.org/10.1086/514291
5. P. Francesconi, Z. Yoti, S. Declich, P. Onek, M. Fabiani, J. Olango, et al., Ebola hemorrhagic fever transmission and risk factors of contacts, uganda, *Emerg. Infect. Dis.*, **9** (2003), 1430–1437. https://doi.org/10.3201/eid0911.030339
6. S. Briand, E. Bertherat, P. Cox, P. Formenty, M. P. Kieny, J. K. Myhre, et al., The international ebola emergency, *N. Engl. J. Med.*, **371** (2014), 1180–1183. https://doi.org/10.1056/NEJMp1409858

7. O. Ilunga Kalenga, M. Moeti, A. Sparrow, V. K. Nguyen, D. Lucey, T. A. Ghebreyesus, The ongoing Ebola epidemic in the Democratic Republic of Congo, 2018–2019, *N. Engl. J. Med.*, **381** (2019), 373–383. https://doi.org/10.1056/NEJMsr1904253
8. D. M. Pigott, N. Golding, A. Mylne, Z. Huang, A. J. Henry, D J Weiss, et al., Mapping the zoonotic niche of Ebola virus disease in Africa, *eLife*, **3** (2014), e04395. https://doi.org/10.7554/eLife.04395
9. E. M. Leroy, B. Kumulungui, X. Pourrut, P. Rouquet, A. Hassanin, P. Yaba, et al., Fruit bats as reservoirs of ebola virus, *Nature*, **438** (2005), 575–576. https://doi.org/10.1038/438575a
10. K. J. Olival, P. R. Hosseini, C. Zambrana-Torrelio, N. Ross, T. L. Bogich, P. Daszak, Host and viral traits predict zoonotic spillover from mammals, *Nature*, **546** (2017), 646–650. https://doi.org/10.1038/nature22975
11. K. E. Jones, N. G. Patel, M. A. Levy, A. Storeygard, D. Balk, J. L. Gittleman, et al., Global trends in emerging infectious diseases, *Nature*, **451** (2008), 990–993. https://doi.org/10.1038/nature06536
12. J. Legrand, R. F. Grais, P. Y. Boelle, A. J. Valleron, A. Flahault, Understanding the dynamics of Ebola epidemics, *Epidemiol. Infect.*, **135** (2007), 610–621. https://doi.org/10.1017/S0950268806007217
13. Z. Q. Xia, S. F. Wang, S. L. Li, L. Y. Huang, W. Y. Zhang, G. Q. Sun, et al., Modeling the transmission dynamics of Ebola virus disease in Liberia, *Sci. Rep.*, **5** (2015) 13857. https://doi.org/10.1038/srep13857
14. D. J. A. Toth, M. Leecaster, W. B. Pettey, A. U. Gundlapalli, H. Gao, J. J. Rainey, et al., The role of heterogeneity in contact timing and duration in network models of influenza spread in schools, *J. R. Soc. Interface*, **12** (2015), 20150279. https://doi.org/10.1098/rsif.2015.0279
15. C. L. Althaus, Estimating the reproduction number of Ebola virus (EBOV) during the 2014 outbreak in West Africa, *PLOS Curr.*, 2014. https://doi.org/10.1371/currents.outbreaks.91afb5e0f279e7f29e7056095255b288
16. G. Chowell, H. Nishiura, Characterizing the transmission dynamics and control of Ebola virus disease, *PLOS Biol.*, **13** (2015), e1002057. https://doi.org/10.1371/journal.pbio.1002057
17. C. M. Rivers, E. T. Lofgren, M. Marathe, S. Eubank, B. L. Lewis, Modeling the impact of interventions on an epidemic of ebola in sierra leone and liberia, *PLOS Curr.*, 2014. https://doi.org/10.1371/currents.outbreaks.4d41fe5d6c05e9df30ddce33c66d084c
18. C. Barril, A. Calsina, J. Ripoll, A practical approach to r_0 in continuous-time ecological models, *Math. Meth. Appl. Sci.*, **41** (2018), 8432–8445. https://doi.org/10.1002/mma.4673
19. D. Breda, F. Florian, J. Ripoll, R. Vermiglio, Efficient numerical computation of the basic reproduction number for structured populations, *J. Comput. Appl. Math.*, **384** (2021), 113165. https://doi.org/10.1016/j.cam.2020.113165
20. Y. Li, L. Wang, L. Pang, S. Liu, The data fitting and optimal control of a hand, foot and mouth disease (HFMD) model with stage structure, *Appl. Math. Comput.*, **276** (2016), 61–74. https://doi.org/10.1016/j.amc.2015.11.090

21. Y. Li, L. W. Wang, Z. H. Peng, H. B. Shen, Basic reproduction number and predicted trends of coronavirus disease 2019 epidemic in the mainland of China, *Infect. Dis. Poverty*, **9** (2020), 94. https://doi.org/10.1186/s40249-020-00704-4

22. M. F. C. Gomes, A. P. y Piontti, L. Rossi, D. Chao, I. Longini, M. E. Halloran, et al., Assessing the international spreading risk associated with the 2014 West African Ebola outbreak, *PLOS Curr.*, 2014. https://doi.org/10.1371/currents.outbreaks.cd818f63d40e24aef769dda7df9e0da5

23. S. Merler, M. Ajelli, A. Vespignani, M. F. C. Gomes, A. P. y Piontti, L. Rossi, et al., Spatiotemporal spread of the 2014 outbreak of Ebola virus disease in Liberia and the effectiveness of non-pharmaceutical interventions: A computational modelling analysis, *Lancet Infect. Dis.*, **15** (2015), 204–211. https://doi.org/10.1016/S1473-3099(14)71074-6

24. J. P. Chretien, S. Riley, D. B. George, Mathematical modeling of the west africa ebola epidemic, *eLife*, **4** (2015), e09186. https://doi.org/10.7554/eLife.09186

25. R. K. Nash, S. Bhatia, C. Morgenstern, P. Doohan, D. Jorgensen, K. McCain, et al., Ebola virus disease mathematical models and epidemiological parameters: A systematic review, *Lancet Infect. Dis.*, **24** (2024), e762–e773. https://doi.org/10.1016/S1473-3099(24)00374-8

26. A. J. Kucharski, A. Camacho, S. Flasche, R. E. Glover, W. J. Edmunds, S. Funk, Measuring the impact of Ebola control measures in Sierra Leone, *Proc. Nat. Acad. Sci.*, **112** (2015), 14366–14371. https://doi.org/10.1073/pnas.1508814112

27. A. Wesolowski, G. Stresman, N. Eagle, J. Stevenson, C. Owaga, E. Marube, et al., Quantifying travel behavior for infectious disease research: a comparison of data from surveys and mobile phones, *Sci. Rep.*, **4** (2014), 5678. https://doi.org/10.1038/srep05678

28. S. Funk, M. Salathé, V. Jansen, Modelling the influence of human behaviour on the spread of infectious diseases, *J. Royal Soc. Interf.*, **7** (2010), 1247–1256. https://doi.org/10.1098/rsif.2010.0142

29. N. Perra, D. Balcan, B. Gonçalves, A. Vespignani, Towards a characterization of behavior–disease models, *PLOS One*, **6** (2011), e23084. https://doi.org/10.1371/journal.pone.0023084

30. S. Funk, E. Gilad, C. Watkins, The spread of awareness and its impact on epidemic outbreaks, *Proc. Nat. Acad. Sci.*, **106** (2009), 6872–6877. https://doi.org/10.1073/pnas.0810762106

31. O. J. Peter, A. I. K. Butt, S. S. S. Ahmad, F. H. H. Al Mukahal, Spatial heterogeneity and nonlinear transmission drive tuberculosis hotspots: a reaction–diffusion modeling study, *AIMS Math.*, **11** (2026), 19400–19439. https://doi.org/10.3934/math.2026788

32. O. J. Peter, A. I. K. Butt, Diffusion-driven pattern formation in a network-based tuberculosis model with higher-order transmission, *Braz. J. Phys.*, **56** (2026), 131. https://doi.org/10.1007/s13538-026-02058-y

33. O. J. Peter, A. I. K. Butt, Diffusion-driven pattern formation in a network-based cholera model with environmental transmission and adaptive mobility, *Ricerche Mat.*, **75** (2026), 1383–1408. https://doi.org/10.1007/s11587-026-01091-y

34. O. J. Peter, Adaptive mobility and zoonotic spillover drive spatial localization in a network-based mpox reaction–diffusion model, *Adv. Cont. Discr. Mod.*, 2026. https://doi.org/10.1186/s13662-026-04111-1

35. A. I. K. Butt, O. J. Peter, A. Kumar, G. B. Balogun, V. A. Adekunle, Fractional-order dynamics of lassa fever: A caputo–fabrizio modelling framework with real statistical data, *Boundary Value Probl.*, **2026** (2026), 114. https://doi.org/10.1186/s13661-026-02319-4

36. A. Wesolowski, T. Qureshi, M. Boni, P. Sundsøy, M. Johansson, S. Rasheed, et al., Impact of human mobility on the emergence of epidemics: Dengue in pakistan, *Proc. Nat. Acad. Sci.,* **112** (2015), 11887–11892. https://doi.org/10.1073/pnas.1504964112

37. J. Varkey, J. Shantha, I. Crozier, C. Kraft, G. Lyon, A. Mehta, et al., Persistence of ebola virus in ocular fluid during convalescence, *N. Engl. J. Med.*, **372** (2015), 2423–2427. https://doi.org/10.1056/NEJMoa1410992

38. E. Leroy, B. Kumulungui, X. Pourrut, P. Rouquet, A. Hassanin, P. Yaba, et al., Multiple ebola virus transmission events and rapid decline of central african wildlife, *Science*, **303** (2004), 387–390. https://doi.org/10.1126/science.1092528

AIMS Press